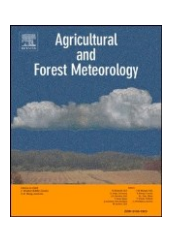


Contents lists available at ScienceDirect

# Agricultural and Forest Meteorology

journal homepage: www.elsevier.com/locate/agrformet





# Eastward shift in *Juniperus virginiana* distribution range under future climate conditions in the Southern Great Plains, United States

Jia Yang\*, Rodney Will, Chris Zou, Lu Zhai, Abigail Winrich, Shanmin Fang

Department of Natural Resource Ecology and Management, Division of Agricultural Sciences and Natural Resources, Oklahoma State University, Stillwater, OK 74078, United States

#### ARTICLEINFO

Keywords:
Woody plain encroachment
Eastern redcedar
Invasive species
Species distribution model Biometeorology
Vegetation composition

#### ABSTRACT

Eastern redcedar (Juniperus virginiana, redcedar) is a major woody species encroaching upon the native grasslands and forests of the southern Great Plains (SGP), representing a significant threat to regional ecosystem services. Future climate change is anticipated to influence redcedar habitat suitability, changing the probability of further encroachment and reshaping its spatial distribution. In this study, we trained seven Species Distribution Models (SDMs) with redcedar records from the USDA Forest Inventory Analysis database and used the ensemble of these SDMs to simulate redcedar distribution probability under current and future climate conditions in Kansas, Oklahoma, and Texas. Results reveal a distinct east-to-west gradient of decreasing distribution probability in the study domain, primarily driven by climate aridity. Throughout the 21st century, the optimal range of aridity for redcedar habitat is projected to shift eastwards by 0.7° (≈ 58 km) under the RCP45 climate scenario and 1.3° (≈ 108 km) under the RCP85. Accordingly, the suitable habitat will shift eastward by 0.6° (≈ 49 km) in the RCP45 and by 1.2° (≈ 103 km) in the RCP85. The proportion of unsuitable habitat will increase from 40.2 % of the study domain during 2000 – 2019 to 48 % in the RCP45 and 54.2 % in the RCP85 during 2080 - 2099. Additionally, highly suitable land areas will decrease from 10.4 % of the study domain during 2000 - 2019 to 1.3 % in the RCP45 and 0 % in the RCP85 by the end of this century. This study suggests a low likelihood of further redcedar encroachment in the west of the SGP states under future climates, while anticipating continued expansion in the east, gradually replacing the existing oak forests and rangelands. The findings provide valuable insights for prioritizing WPE management resources and contribute to our understanding of future changes in the SGP vegetation composition and their impacts on ecosystem dynamics.

#### 1. Introduction

Woody Plant Encroachment (WPE) is a widespread phenomenon observed globally in various regions, including Africa (Venter et al., 2018), Australia (Stevens et al., 2017), South America (Anadon et al., '2014), and North America (Filippelli et al., 2020; Saintilan and Rogers, 2015). In the southern Great Plains (SGP) of the United States including Kansas, Oklahoma, and Texas, WPE is occurring at an alarming rate of over 1 % land cover change per year, which is five to seven times faster than in other regions of the nation (Archer et al., 2017; Barger et al., 2011; Wilcox et al., 2018). Eastern redcedar (*Juniperus virginiana*), a native woody species to eastern North America, has become the primary encroaching woody species upon the native grasslands and forests of the SGP. Over the past four decades, the encroachment of eastern redcedar has transformed Oklahoma grasslands into juniper woodlands at a rate of approximately 40 km² per year (Wang et al., 2018).

The encroachment of eastern redcedar is causing a range of adverse impacts on grassland ecosystems, such as the reduction in grassland productivity, livestock carrying capacity, ecosystem water yield, and wildlife habitat quality (Archer et al., 2017). Anadon et al. (2014) ' estimated that a 1 % increase in woody plant coverage can cause a decrease in grassland net primary productivity of 41 g C  $m^{-2}$ yr $^{-1}$ and reduce livestock production by 0.6

to 1.6 cows km<sup>-2</sup>. Moreover, WPE can affect the water dynamics of ecosystems. Studies by Zou et al. (2018) showed that WPE influences all components of the water budget in affected areas. Woody plants exhibit higher rates of evapotranspiration and rainfall interception compared to herbaceous species, resulting in reduced runoff generation and streamflow (Huxman et al., 2005; Kishawi et al., 2023; Qiao et al., 2017). Furthermore, the encroachment of eastern redcedar in the SGP has resulted in the loss of habitat for grassland-associated wildlife species (Thompson et al., 2014) and an increase in the transmission of vector-borne diseases (Loss et al., 2022).

The encroachment of eastern redcedar into oak-dominated forests is having significant impacts on forest structure and functions in the eastern SGP (Hoff et al., 2018b; Torquato et al., 2020b). In the Cross Timbers forest matrix of Oklahoma, it has been estimated that encroached eastern redcedar trees in the midstory and understory have aboveground biomass of 6.3 Mg ha<sup>-1</sup>, representing a 38 % increase in available wildfire fuel loads within the existing forest stands (Hoff et al., 2018b). As a result, the presence of eastern redcedar under oak tree canopy exacerbates forest flammability and creates more ladder fuels in the forests (Hoff et al., 2018b), which in turn raises the probability of catastrophic wildfires. In the SGP, eastern redcedar trees have a competitive advantage over many deciduous tree species due to their

relatively high drought tolerance (Torquato et al., 2020a). If left unchecked, they have the potential to replace native deciduous forests, resulting in a reduction in ecosystem biodiversity (Meneguzzo and Liknes, 2015) and constraining the growth of grasses beneath their canopies (Bennion and Ward, 2022).

The encroachment of eastern redcedar in the SGP can be attributed to a number of natural and anthropogenic factors, including changes in precipitation patterns, fire exclusion and suppression, and overgrazing (Archer et al., 2017). Annual average precipitation is a critical factor in determining the boundary between grasslands and woody plants, as well as the upper limit of woody plant fraction (Sankaran et al., 2005; X. Yang et al., 2023). Over the past three decades, the SGP has experienced a wetter-than-average period, with Oklahoma having the wettest two decades in the 1990s and the 2010s (Kunkel, 2022). This above-average precipitation may have contributed to the expanded range of eastern redcedar. Notably, as the SGP is expected to become drier and warmer in the future, the mortality rates of eastern redcedar trees may increase, potentially limiting their expansion and leading to the redistribution in the SGP (Breshears et al., 2005; Twidwell et al., 2014). However, the redistribution has not been rigorously examined in previous studies and become a critical knowledge gap in the predictive understanding of redcedar dynamics. Prior to European settlement, the grasslands in the SGP were maintained by a feedback loop between fine fuel and low-intensity fires that had been occurring for thousands of years (Pyne, 2017, 1984). Along with the aggressive fire exclusion and suppression policies in the 20th century, the feedback was disrupted, resulting in a significant increase in woody plant coverage (Fuhlendorf et al., 2008; Wilcox et al., 2018). Additionally, the introduction of large herds of domestic livestock (Box, 1967) reduced the frequency of wildfires and promoted the proliferation of woody plant species (Fuhlendorf et al., 2008).

Various management practices have been used to control the redcedar expansion. During the 1960s and 1970s, brush management such as mechanical removal and herbicide injection began to be implemented to control the encroachment of woody plants in the SGP (Archer and Predick, 2014). However, these methods are labor-intensive and have limited longterm effectiveness, typically lasting less than 10 years (Scholtz et al., 2021). Currently, the most effective strategy for controlling redcedar encroachment in grasslands is the reintroduction of fire and the reestablishment of fine fuel (Wilcox et al., 2018). Utilization of prescribed burning must be carefully planned, taking into consideration the condition of the redcedar trees and the critical fire intensity-mortality threshold. Twidwell et al. (2013a) found that redcedar trees up to a height of 4.5 m can be killed when fire line intensity exceeds 160 kW  $m^{-1}$ .

Due to the existence of varying control practices, the current distribution of redcedar may not accurately portray its complete potential for encroachment. Moreover, the suitability of its habitat can undergo significant

changes in response to future climate conditions. To effectively devise proactive conservation and management strategies aimed at mitigating its expansion, particularly in areas of high conservation significance and those serving as vital watersheds, a comprehensive understanding of the most susceptible habitats for redcedar encroachment is crucial. Additionally, it is essential to anticipate how the range of this encroachment-prone species will evolve in response to future climate shifts. By acquiring such knowledge, conservationists and land managers can implement targeted measures to preserve valuable ecosystems and safeguard water resources.

Species Distribution Models (SDMs) are valuable tools for predicting the potential distribution of plant and animal species by examining the relationship between species occurrence and environmental factors, based on the concept of a species' ecological niche (Miller, 2010). They are increasingly being used to support management decisions related to biodiversity, biogeography, and natural resources (Guillera-Arroita et al., 2015). Over the last two decades, modeling algorithms and software packages for simulating species distribution have advanced significantly. Commonly used modeling methods include but are not limited to the Maximum Entropy model (MaxEnt) (Phillips et al., 2009; Phillips and Dudík, 2008), Generalized Linear Model (GLM) and Generalized Additive Model (GAM) (Guisan et al., 2002), and Random Forest (RF) (Evans et al., 2011). These SDMs have been extensively tested and used for predicting species distributions in future periods (e.g. Mainali et al., 2015; Remya et al., 2015; Wei et al., 2018). It is known that every single SDM has advantages as well as limitations in its spatial projection (Lissovsky and Dudov, 2021). Model ensemble approach that incorporates multiple SDMs (such as Generalized Linear Model, Random Forest, and MaxEnt) takes advantage of the strengths of different modeling techniques and reduces the biases in any individual model, resulting in more robust estimates of habitat suitability (Shabani et al., 2016). This study had two objectives: (1) training SDMs using eastern redcedar records from the USDA Forest Inventory Analysis (FIA) data to simulate the spatial pattern of distribution probability under current climate conditions in the SGP; and (2) simulating temporal and spatial changes in distribution probability for eastern redcedar trees under future climate change scenarios. Environmental factors to drive the model include climate, topography, soil texture and property variables. The anticipated climate warming and drying in the SGP in the 21st century (Modala et al., 2017; J. Yang et al., 2023) are expected to have significant impacts on habitat suitability and distribution of eastern redcedar. By examining these potential changes, this study provides valuable insights for government agencies and landowners in making informed decisions regarding the management of woody plant encroachment. Furthermore, the results of this study can contribute to our understanding of future changes in vegetation composition in the SGP and their impacts on ecosystem biophysical and biogeochemical processes.

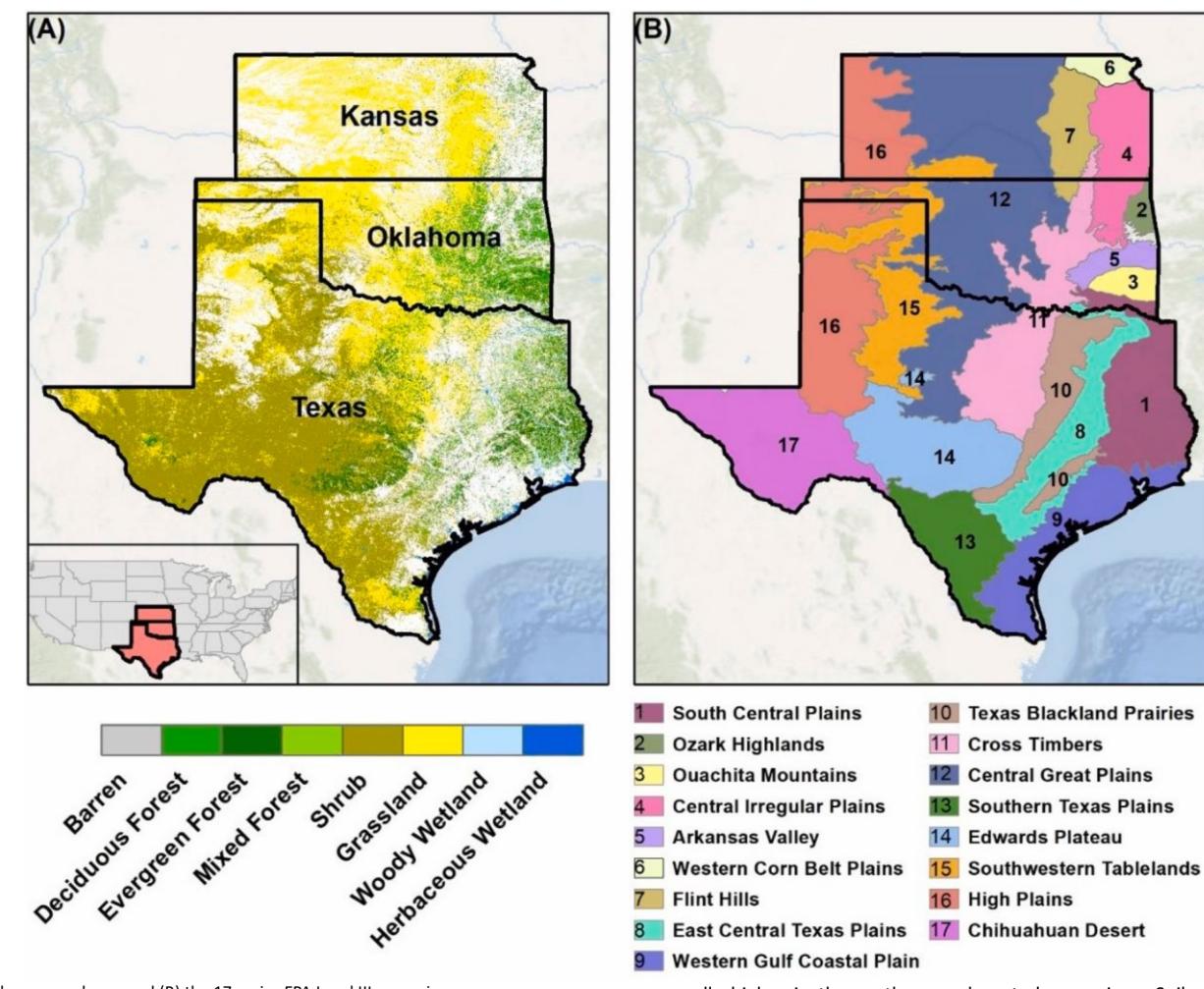
#### 2. Materials and methods

#### 2.1. Study domain

The study area encompasses the three SGP states of Kansas, Oklahoma, and Texas (Fig. 1A). The focus of this study is the three states excluding the highly managed areas of croplands, pasture, and urban. It is assumed that, if climate permits, eastern redcedar can potentially grow in barren land, forests, shrublands, grasslands, and wetlands in the SGP, which were identified from the 2019 land cover map in the National Land Cover Database (NLCD) (Homer et al., 2012). The study area covers a total of 0.82 million km<sup>2</sup>, with forests, shrubs, grasslands, wetlands, and barren land accounting for 17.8 %, 42.5 %, 35.1 %, 4.2 %, and 0.4 %, respectively. The study domain encompassed of 17 ecoregions, namely the South Central Plains, Ozark Highlands, Ouachita Mountains, Central Irregular Plains, Arkansas Valley, Western Corn Belt Plains, Flint Hills, Eastern Central Texas Plains, Western Gulf Coastal Plain, Texas Blackland Prairies, Cross Timbers, Central Great Plains, Southern Texas Plains, Edwards Plateau, Southwestern Tablelands, High Plains, and Chihuahuan Fig. 1. Study domain of the three states in the southern Great Plains, encompassing Kansas, Oklahoma, and Texas. (A) Land cover types in the three states excluding

Desert (Fig. 1B).

Figure S1 provides an overview of the climate characteristics of the



the highly managed area and (B) the 17 major EPA Level III ecoregions.

study domain during 2000 – 2019, based on the gridMET dataset (Abatzoglou, 2013). The average annual temperature shows a north-to-south increasing gradient, while annual precipitation and the Aridity Index (AI, calculated as the ratio of 20-year average annual precipitation to potential evapotranspiration) exhibit an east-to-west decreasing gradient. Over the 20 years, the study domain had an average annual temperature of 17.0 °C. The Southern Texas Plains and Western Gulf Coastal Plain ecoregions had the highest annual temperature, reaching 22.1 °C and 22.0 °C, respectively, while the Western Corn Belt Plains and Flint Hills ecoregions had the lowest, at 12.2 °C and 13.4 °C, respectively (Table S1). The average annual precipitation in the study domain was 765 mm, with the South Central Plains and Ouachita Mountains ecoregions receiving the highest amount at 1298 mm and 1300 mm, respectively. In contrast, the Chihuahuan Desert and the High Plains ecoregions had the lowest precipitation, with values of 345 mm and 471 mm, respectively. The AI values ranged from 0.22 in the Chihuahuan Desert to 0.97 in the Ouachita Mountains. Using the AI-based climate classification scheme (Middleton and Thomas, 1997), five ecoregions were within the semi-arid climate zone, two ecoregions were in the sub-humid climate zone, and ten ecoregions were in the humid climate zone.

Elevation in the study domain generally increases from east to west, ranging from less than 200 m to over 1200 m (Figure S2). The East Central Texas Plains (28 m) and the South Central Plains (93 m) are the ecoregions with the lowest elevation, while High Plains (1017 m) and Chihuahuan Desert (1097 m) have the highest elevation. Spatial variations in soil texture and properties are evident in the study domain (Figure S3). The percentage of sand in soil is higher in the southeast and southwest ecoregions, such as the South Central Plains and the Chihuahuan Desert. The percentages of silt and clay are

generally higher in the northern and central ecoregions. Soil pH shows a gradual transition from acidic in the east (pH < 6.5), to neutral in the central (6.5 < pH < 7.5), and alkaline in the west (pH > 7.5), which aligns with the changing pattern of annual precipitation. Soil bulk density tends to be greater in ecoregions in the central and southern parts (> 1.45 g cm $^{-3}$ ) than those in the eastern and northern parts (< 1.45 g cm $^{-3}$ ).

## 2.2. Species distribution models

In this study, we used the "biomod2" R package (Thuiller et al., 2023) to train seven SDMs and construct the ensemble model. The seven SDMs include Artificial Neural Network (ANN), Flexible Discriminant Analysis (FDA), Generalized Additive Model (GAM), Generalized Boosting Model (GBM), Generalized Linear Model (GLM), MaxEnt, and Random Forest (RF). All of these models have been previously used to predict the probability of species distribution based on the relationship between environmental conditions and species presence records (e.g. Elith et al., 2011; Franklin, 2010). They have also been used to project changes in habitat suitability under future climate conditions (e.g. Remya et al., 2015; Wei et al., 2018; Zhou et al., 2021). In this study, we used the seven SDMs to simulate the spatial pattern of eastern redcedar's distribution probability at a spatial resolution of 0.005° over the contemporary period (2000 – 2019) and four future periods (i.e., 2020 – 2039, 2040 – 2059, 2060 – 2079, and 2080 – 2099).

It should be noted that the extent of model simulations in this study was larger than the study domain, encompassing both the three SGP states (i.e., Kansas, Oklahoma, and Texas) and three additional states to the east (i.e., Missouri, Arkansas, and Louisiana) and two states to the west (i.e., Colorado and New Mexico) (Fig. 2). The inclusion of these additional states provided a larger sample size of eastern redcedar records and a greater range of

environmental conditions during the model training process. SDMs can suffer from reduced accuracy when making future projections due to environmental variables, particularly future climate conditions, being outside the range of conditions encountered during model training (Merow et al., 2013; Phillips, 2005). Therefore, we expanded the spatial extent of model simulations to increase the range of climate conditions during model training and improve model transferability to future climate conditions.

#### 2.3. Data preparation for species distribution models

#### 2.3.1. Records of eastern redcedar trees

The locations of eastern redcedar samples were obtained from the dataset of the USDA Forest Inventory and Analysis (FIA) National Program. Raw FIA data for the eight states were downloaded from the FIA DataMart (https://apps.fs.usda.gov/fia/datamart/datamart.html). Using the species code (068), we selected tree records of eastern redcedar that were inventoried after the year of 2000 and linked them to their respective plot records to extract their geographic coordinates.

In the public release version of the FIA data, plot coordinates are rounded to the nearest 100 'onds to protect landowners' privacy. This rounding can result in errors in tree plot coordinates of up to 1.6 km and lead to uncertainties in their associated environmental conditions with fast spatial changes, such as topography. To mitigate this potential error, an adjustment process was implemented using Google Earth Pro, as illustrated in Fig. 3. First, we created a buffer zone (circle polygon with a radius of 1.6 km) around each FIA plot. Then, we used high-resolution satellite remote sensing imageries

from multiple years and different seasons to visually identify areas containing eastern redcedar trees within each buffer zone. Winter imagery was found to be particularly useful for identifying redcedar trees when deciduous trees were dormant. Finally, the original FIA plots were moved to their new locations based on the identified redcedar areas (as shown by the cyan pinpoint being relocated to the magenta pinpoint in Fig. 3). This process was repeated for all these selected FIA plots in the model simulation domain. It is possible that there were more than one redcedar stands within one buffer zone. In that case, we selected the larger stand and moved the FIA plot to the centroid of that stand.

In the process of adjusting the redcedar plot locations using satellite imageries, there were cases where eastern redcedar trees could not be identified within their buffer zones. This could be attributed to human management practices or land disturbances such as wildfires that cleared the forest stands. These plots were excluded from the sample dataset and were not used for model training. Furthermore, there were challenges in differentiating eastern redcedar trees from other evergreen trees from satellite imageries, particularly in pine plantation areas. These plots were also excluded from the model training samples. Ultimately, we obtained a total of 3378 eastern redcedar plots with corrected coordinate information (Fig. 2). These plots were distributed across six states, with 1060 in Missouri, 856 in Arkansas, 77 in Louisiana, 139 in Kansas, 720 in Oklahoma, and 526 in Texas. Although there was no FIA eastern redcedar plots in New Mexico and Colorado (Fig. 2),

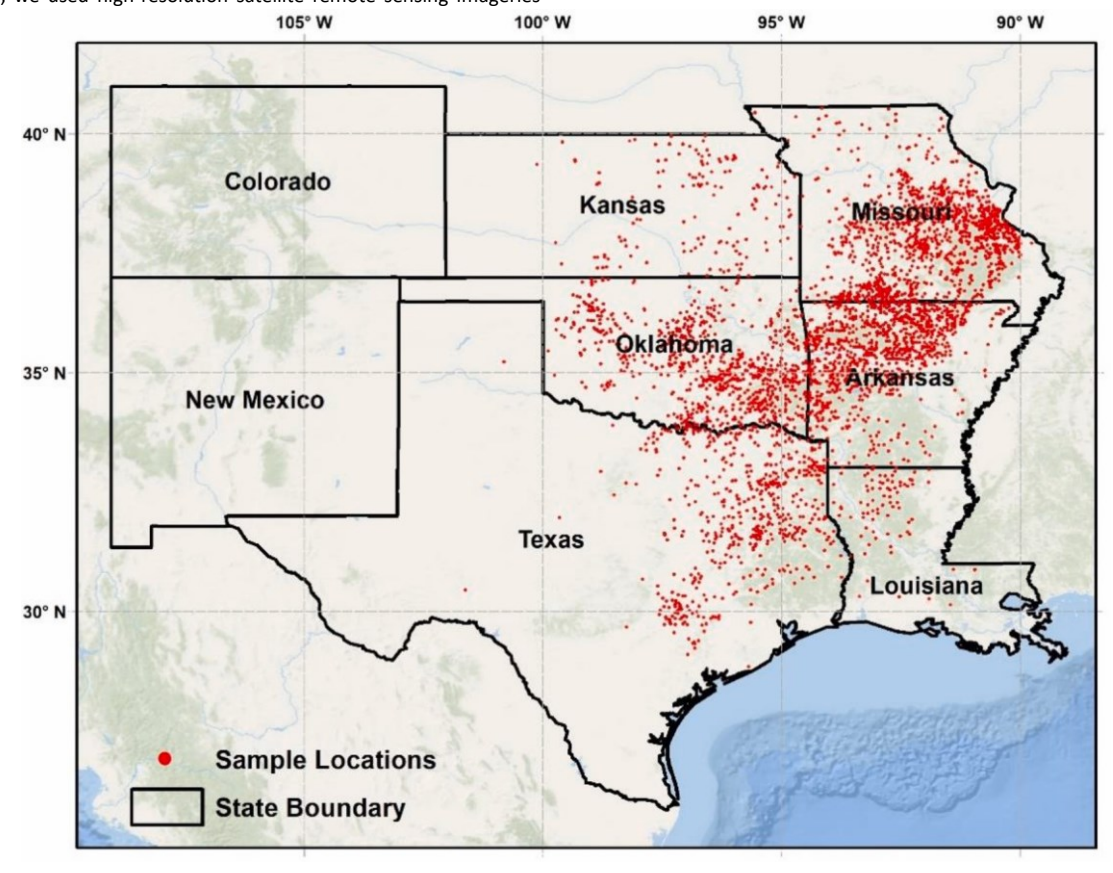


Fig. 2. Model simulation extent, which covers eight states in the southern U.S. including the three states in the southern Great Plains (Kansas, Oklahoma, Texas), as well as three states to the east (Missouri, Arkansas, and Louisiana) and two states to the west (Colorado and New Mexico). The red dots on the map denote the locations of eastern redcedar plots in the eight states, modified based on the records from the USDA Forest Inventory and Analysis (FIA) National Program.

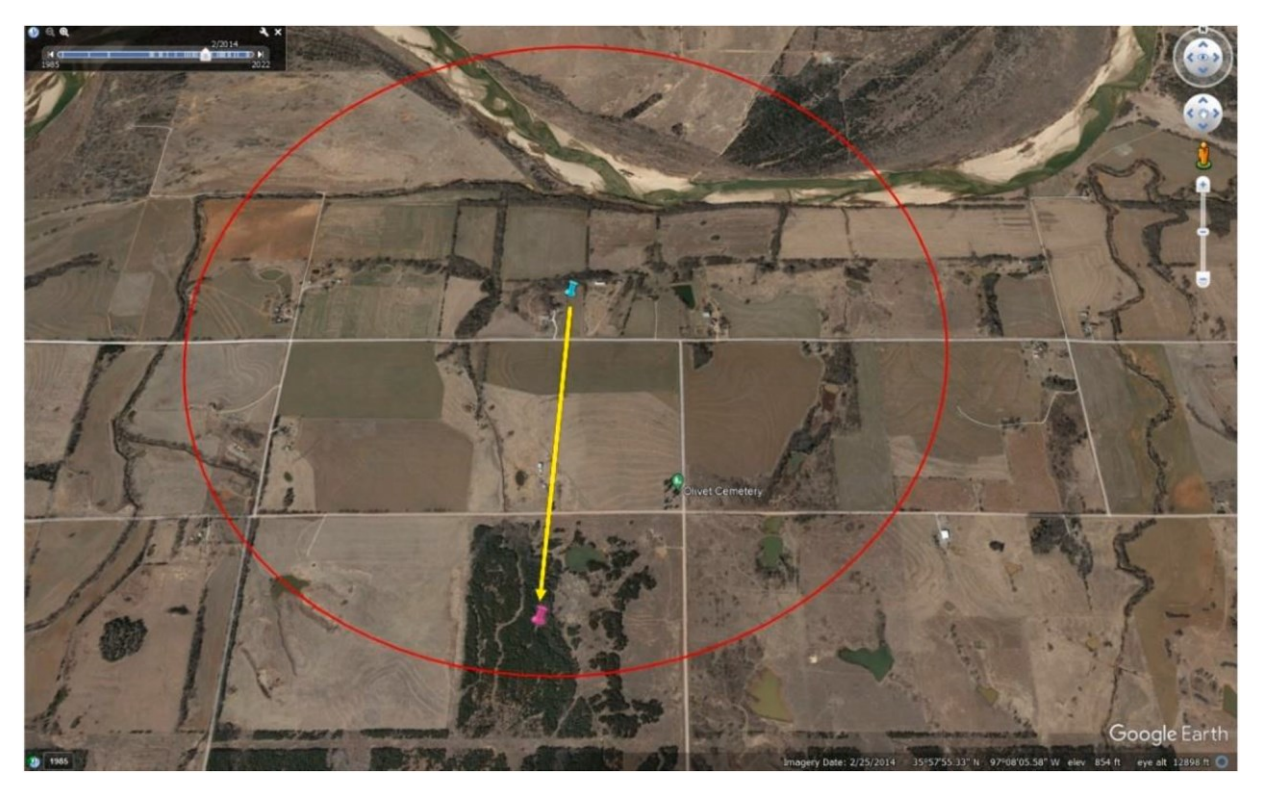


Fig. 3. An example of the adjustment of FIA plot using Google Earth Pro. In this example, the redcedar plot is located in Payne County, Oklahoma (35°57′, 97°06′). The high-resolution satellite image was captured on February 25, 2014. The original plot location is marked by the cyan pinpoint, while the magenta pinpoint indicates the adjusted location. The red circle is the created buffer zone with a radius of 1.6 km around the plot.

the two states were still included in the model simulation to enable SDMs to select background points and expand the range of climate conditions during the training process.

#### 2.3.2. Potential predictor variables

To drive the model, we utilized three types of environmental factors: climate conditions, topography, and soil texture and properties, all of which are known to influence the distribution of eastern redcedar trees (Bennion, 2023). These predictor factors covered the eight states of the model simulation domain (Fig. 2) and were downscaled/upscaled to a spatial resolution of 0.005° for model simulations.

Climate data were prepared for five 20-year periods in the 21st century, i.e., 2000 – 2019, 2020 – 2039, 2040 – 2059, 2060 – 2079, and 2080 – 2099. Climate data during 2000 – 2019 were obtained from the gridMET data (Abatzoglou, 2013), which provides daily surface meteorological data in the contiguous U.S. at a spatial resolution of approximately 4 km. For the four future 20-year periods, climate data were from the downscaled General Circulation Model (GCM) simulation results under two Representative Concentration Pathways of the RCP45 and RCP85 scenarios in the CMIP5 (Taylor et al., 2012). To account for the divergence in the projected climate conditions by GCMs, we used climate data simulated by seven GCMs, including BCC–CSM1, CCSM4, GFDL-ESM2G, HadGEM2-ES365, IPSL-CM5A-LR, MIROC5, and

NorESM1-M. These data had been downscaled to a spatial resolution of 4 km and bias-corrected according to the gridMET historical climate data using the Multivariate Adaptive Constructed Analogs (MACA) developed by Abatzoglou and Brow (2012).

Six climate factors were considered as potential predictors for SDM simulations. These factors included the 20-year average temperature ( $T_{avg}$ , °C), 20-year average hottest month temperature ( $T_{hotmonth}$ , °C), the average diurnal temperature range ( $T_{range}$ , °C), the number of days each year with a daily minimum temperature greater than 0 °C ( $N_{tmin}$ >0), the average annual precipitation ( $P_{onn}$ , mm), and the Aridity Index (AI). AI was calculated

as the ratio of annual precipitation to potential evapotranspiration, which was determined using the Priestley-Taylor equation (Priestley and Taylor, 1972).

Topographic variables of slope and aspect were included in the SDMs as potential predictors, which were derived from the 90-m Multi-Error-Removed Improved-Terrain DEM (MERIT DEM) (Yamazaki et al., 2017). Slope and aspect were calculated using ArcToolbox in ArcGIS 10.8. The aspect was further categorized into eight directions: North, Northeast, East, Southeast, South, Southwest, West, and Northwest. We also processed the 250-m SoilGrid data (Poggio et al., 2021) to obtain five types of soil texture and properties in the topsoil layer. These five types of soil data included the percentages of sand (sand%), silt (silt%), and clay (clay%), soil bulk density (bulkden, g cm<sup>-3</sup>), and soil pH value.

### 2.3.3. Feature selection

Multicollinearity among predictor variables can impact parameter estimation by inflating the variance of regression parameters and leading to inaccurate identification of relevant predictors (Dormann et al., 2013). While some SDMs, such as MaxEnt and RF, are generally resilient to predictor collinearity during model training, the shift in collinearity under novel climate conditions can reduce model transferability (Feng et al., 2019). To address the issue of multicollinearity, we calculated the variance inflation factor (VIF) for the potential climate, topographic, and soil predictor variables in the 3378 redcedar plots. Predictor variables with a VIF greater than 5 were excluded. In the end, we selected nine predictor variables for model training and future prediction, which were T<sub>avg</sub>, T<sub>range</sub>, AI, slope, aspect, sand%, clay%, bulkden, and pH (Table 1). Noted that Thotmonth, Pann, Ntmin>0, and silt% were not included in the model due to their high correlation with AI, Tavg, sand%, and clay%. This exclusion helps mitigate potential redundancy in the model, ensuring the selected variables capture distinct information and improve model performance. Additionally, the removal of multicollinearity ensures the marginal response curve can effectively reflect the response of habitat suitability to environmental factors (see Section 2.5).

**Table 1**The calculated variance inflation factor (VIF) for predictor variables before and after feature selection.

Predictor	VIF before feature selection	VIF after feature selection variables
T <sub>ovg</sub> *	517.3	3.1
T <sub>hot month</sub>	26.6	Not selected
Trange *	20.9	1.5
Vtmin>0	336.0	Not selected
Pann	339.5	Not selected
A/ *	436.9	4.1
slope *	1.3	1.2
aspect *	1.0	1.0
and% *	$2.1 \times 10^{14}$	3.5
ilt%	$1.7 \times 10^{14}$	Not selected
clay% *	$3.7 \times 10^{13}$	2.4
oulkden *	3.8	3.8
о <b>Н</b> *	3.2	3.0

Note:

#### 2.4. Model settings and simulations

In this study, we employed the function in biomod2 to randomly select 4000 pseudo-absences. The FIA eastern redcedar plots and pseudo-absences were then randomly partitioned into a training dataset (80 % of the data) and an independent testing dataset (the remaining 20 %). To enhance the robustness of our simulation results, this process was repeated five times. Subsequently, we tuned the model options for each SDM. For the GLM, we opted for the "Quadratic" model form and set the interaction level to "1" to account for the interactions between environmental factors. For the GBM, the parameter "n.trees" was set to 1000. For the GAM, we utilized the "GAM\_mgcv" function to fit the model. RF was configured with "ntrees" set to 1000 and "nodesize" set to 5. For ANN, the number of cross validations to identify the best size and decay parameters ("ncCV") was set to 5 and the maximum number of model iterations ("maxit") was set to 200. For FDA, we chose the multivariate adaptive regression splines ("MARS") as the regression method in optimal scaling. For MaxEnt, four feature functions including "linear features", "quadratic features", "threshold features", and "hinge features" were selected to allow MaxEnt to automatically use the "best" feature function based on the sample size. We tuned the "Regularization multiplier" parameter and set it to 2 (Radosavljevic and Anderson, 2014).

We conducted simulations in the contemporary period (2000 – 2019) to obtain distribution probability maps from the outputs of each SDMs and the ensemble model and assess the performance of the SDMs. Model performance was evaluated using the area under the receiver operating characteristic (ROC) curve (AUC), which is a popular metric to evaluate the performance of SDMs in distinguishing between species presence and background samples. After model evaluation, we used the ensemble model to generate redcedar distribution probability maps in the contemporary period and four future periods in the RCP45 and RCP85 scenarios.

Although we expanded the simulation domain to encompass a broader range of climate conditions, it is possible that future climate in the three SGP states falls outside the current climate range. For future projections, we performed a Multivariate Environmental Similarity Surface (MESS) analysis to assess the degree of similarity or dissimilarity in environmental conditions between the model training and projection processes (Elith et al., 2010). The MES values range from – 100 % to 100 %. Negative MES values indicate that

the predictors in the projection process are beyond the range of the reference training data, while positive values indicate a larger similarity between the reference data and the predictors in the projection process (Polce et al., 2014). A MES value of 100 % indicates the set of environmental factors is identical to those in the training process. Additionally, we identified the Most Dissimilar Variable (MDV) among the selected predictor variables for grids with negative MES values. The algorithm to calculate MES and identify MDV can be found in the Online Supplementary Material of Elith et al. (2010). The MESS analysis and MDV identification are useful to understand the potential limitations and model reliability associated with projecting redcedar habitat suitability under future climate conditions.

Model simulations were conducted in each of the five 20-year periods of  $2000-2019,\,2020-2039,\,2040-2059,\,2060-2079,\,$  and 2080-2099 using the ensemble model of the seven SDMs. For the four future periods, climate data were obtained from the simulations conducted by seven GCMs in the RCP45 and the RCP85 scenarios (see the description in 2.3.2). In total, the ensemble model was used to perform 56 simulations for the future periods (4 future periods  $\times$  7 GCMs  $\times$  2 scenarios). 2.5. Analyses

We conducted permutation tests to assess the relative importance of the nine selected environmental variables in each SDM and the ensemble model. The permutation test involved randomly permuting the values of each environmental variable for both the training presence data and pseudoabsences and then refitting the SDMs using the permuted values. The resulting decrease in AUC for each variable was normalized to percentages to represent their relative importance in the model.

The marginal response curves were generated to examine the response of the simulated eastern redcedar distribution probability to environmental factors. These curves could be misleading if the environmental variables are highly correlated. However, as we have already addressed the issue of multicollinearity by removing highly correlated variables (Section 2.3.3), the marginal response curves can effectively demonstrate the responses. To focus on the most influential variables, we created response curves only for the environmental factors with permutation importance greater than 10 % in the ensemble model.

The simulated distribution probability ranges from 0 to 1. To facilitate result interpretation and analysis, we categorized these probability values into four habitat suitability classes: unsuitable habitat (0-0.05), poorly suitable habitat (0.05-0.33), moderately suitable habitat (0.33-0.67), and highly suitable habitat (0.67-1) (Wei et al., 2018). Finally, we analyzed the spatial pattern of redcedar habitat suitability and assessed how it would change under future climate conditions.

#### 3. Results

### 3.1. Model evaluation and variable contributions

Fig. 4 shows the simulated spatial pattern of the distribution probability of eastern redcedar by seven distribution models in the period of 2000 – 2019 and their ensemble results. All these models simulated a higher distribution probability in the eastern part of the SGP, which is consistent with the spatial pattern of FIA redcedar plots in Fig. 2. The boxplot in Fig. 5 shows the average AUC and AUC variations of the five replications for each of the seven selected SDMs. In terms of the average AUC of five replications, ANN had the lowest average AUC of 0.868. The other six SDMs had an average AUC over 0.9, which was 0.901 for FDA, 0.904 for GAM, 0.909 for GBM, 0.908 for GLM, 0.908 for MaxEnt, and 0.911 for RF. The high AUC values indicate that all seven models, along with the selected predictor variables, effectively captured the spatial distribution of eastern redcedar distribution probability during the contemporary period. It also provides confidence in the ability of model ensemble approach to predict redcedar distribution probability under future climate conditions.

The results of the permutation test indicate the relative importance of environmental factors in shaping the spatial pattern of eastern redcedar

<sup>\*</sup>refers to the predictor variables selected for model training and future projection.

distribution probability (Table 2). According to the results of the seven SDMs and the ensemble model, climate variables were identified as the most influential factors. In the ensemble model, AI was associated

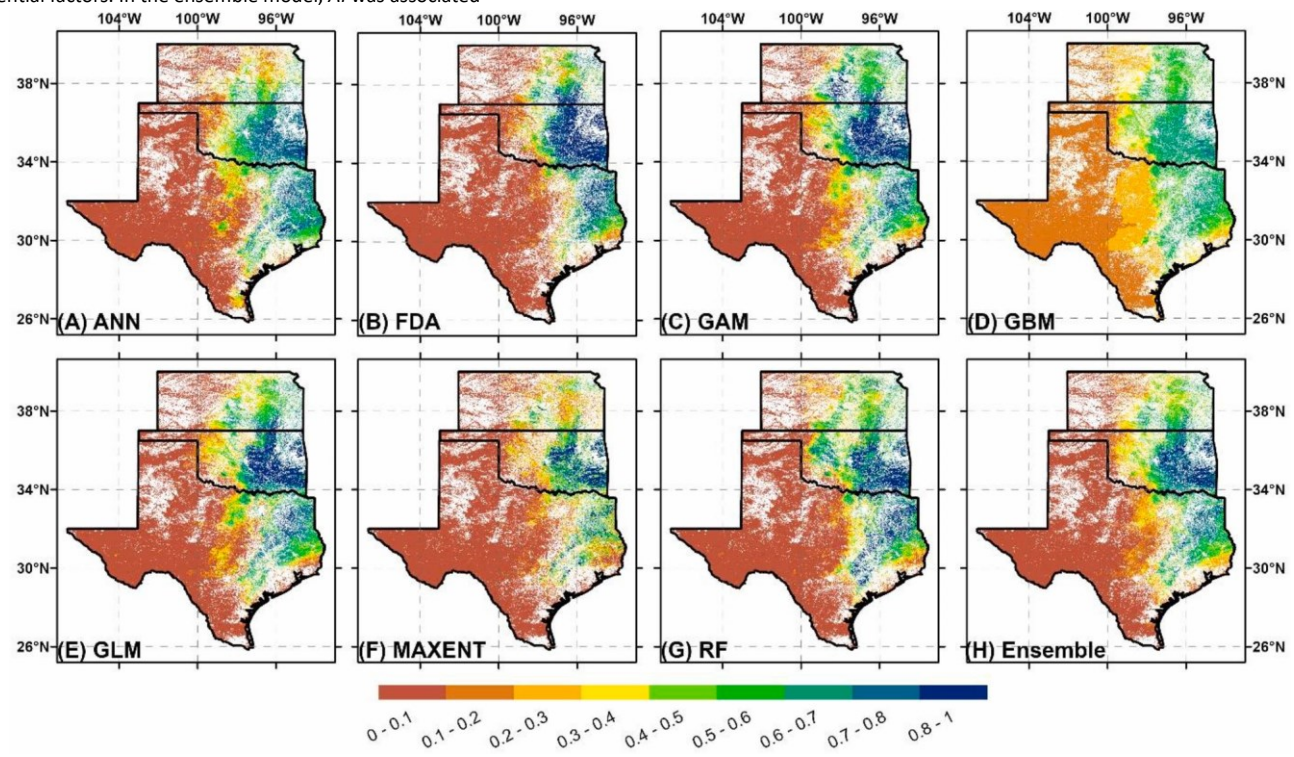


Fig. 4. The simulated distribution probability of eastern redcedar by seven species distribution models (A - G) in the contemporary period and their ensemble results (H). (A) ANN: Artificial Neural Network, (B) FDA: Flexible Discriminant Analysis, (C) GAM: Generalized Additive Model, (D) GBM: Generalized Boosting Model, (E) GLM: Generalized Linear Model, (F) MaxEnt: Maximum Entropy, and (G) RF: Random Forest.

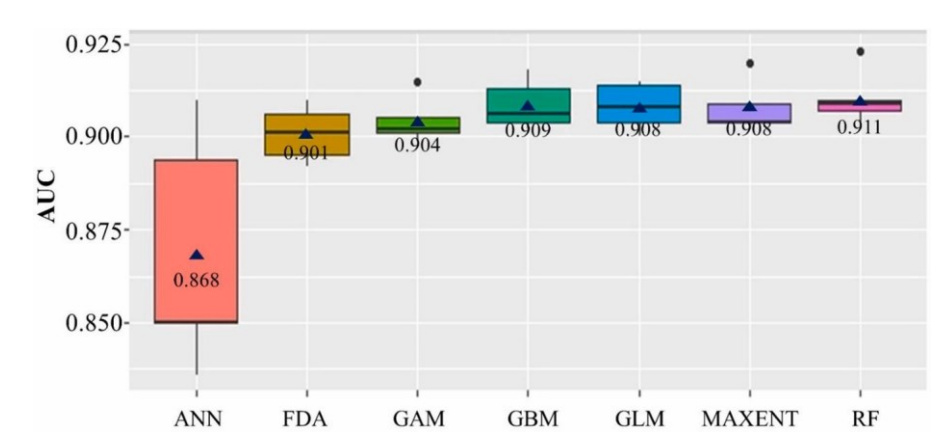


Fig. 5. The area under the receiver operating characteristic curve (AUC) for evaluating the performance of seven species distribution models in simulating the spatial distribution of eastern redcedar in the southern Great Plains. Boxplot is used to show the distribution of AUC of five model replications and triangles in the boxplot show the average AUC of the five replications. ANN: Artificial Neural Network, FDA: Flexible Discriminant Analysis, GAM: Generalized Additive Model, GBM: Generalized Boosting Model, GLM: Generalized Linear Model, MaxEnt: Maximum Entropy, and RF: Random Forest.

 Table 2

 The normalized permutation importance for the nine predictor variables in the seven species distribution models (ANN, FDA, GAM, GBM, GLM, Maxent, and RF) and the ensemble model.

	ANN	FDA	GAM	GBM	GLM	MaxEnt	RF	Ensemble
AI	30.2 %	81.0 %	69.8 %	85.9 %	49.2 %	52.2 %	50.1 %	69.9 %
bulkden	4.2 %	2.6 %	1.5 %	3.4 %	4.4 %	3.0 %	4.8 %	1.9 %
clay%	9.5 %	2.7 %	1.4 %	1.2 %	1.1 %	3.4 %	4.0 %	2.1 %
aspect	0.0 %	0.0 %	0.0 %	0.0 %	0.0 %	0.1 %	0.2 %	0.0 %
pН	22.5 %	0.5 %	0.4 %	0.1 %	6.1 %	3.3 %	6.5 %	2.6 %
sand%	9.4 %	1.0 %	3.5 %	0.1 %	7.0 %	6.2 %	4.2 %	2.5 %
slope	1.6 %	3.2 %	1.6 %	3.5 %	1.7 %	7.8 %	6.4 %	2.6 %
Tavg	19.5 %	8.9 %	21.3 %	5.8 %	23.8 %	22.5 %	19.6 %	17.8 %
Trange	3.1 %	0.1 %	0.4 %	0.0 %	6.6 %	1.4 %	4.3 %	0.8 %

with the highest importance of 69.9 %, followed by  $T_{avg}$  with an importance of 17.8 %. Among the non-climate environmental factors, pH and slope exhibited the highest importance with a permutation importance value of 2.6 %. Additionally, sand%, clay%, and bulkden had an importance value of 2.5 %, 2.1 %, and 1.9 %, respectively. This indicates soil properties and topography had a relatively lower but still noticeable contribution to the spatial pattern of distribution probability.

Fig. 6 displays the responses of simulated relative habitat suitability to the most important environmental factors of AI and  $T_{avg}$  in the ensemble model. Habitat suitability initially increases with AI within the range of 0 to 0.9. However, in a humid environment where AI exceeds 0.9, habitat suitability starts to decline. The optimal AI range for eastern redcedar habitat (distribution probability > 0.67) lies between 0.6 and 1.25. For  $T_{avg}$ , redcedar habitat suitability increases with  $T_{avg}$  in regions with relatively low temperature ( $T_{avg} < 13~^{\circ}C$ ) and decreases with  $T_{avg}$  in regions with relatively high temperature ( $T_{avg} > 16~^{\circ}C$ ). The optimal  $T_{avg}$  range for eastern redcedar habitat (distribution probability > 0.67) falls between 11  $^{\circ}C$  and 18.6  $^{\circ}C$ . By considering the climate statistics in each ecoregion (Table S1), it is observed that seven ecoregions had average climate conditions within the optimal ranges for both AI and  $T_{avg}$ . These ecoregions were Ozark Highlands (AI = 0.94,  $T_{avg} =$ 

15.5 °C), Ouachita Mountains (AI = 0.97,  $T_{avg} = 16.4$  °C), Central Irregular Plains (AI = 0.88,  $T_{avg} = 14.3$  °C), Arkansas Valley (AI = 0.88,  $T_{avg} = 16.7$  °C), Western Corn Belt Plains (AI = 0.78,  $T_{avg} = 12.2$  °C), Flint Hills (AI = 0.76,  $T_{avg} = 13.4$  °C), and Cross Timbers (AI = 0.65,  $T_{avg} = 17.6$  °C).

#### 3.2. Future shift in optimal climate conditions

According to the future climate statistics in Tables S2 and S3, the SGP and all 17 ecoregions will have a warming and drying trend in both the RCP45 and RCP85 scenarios. In the RCP45, the annual temperature for the entire study domain is projected to increase from 17.0 °C in 2000 – 2019 to 19.6  $\pm$  0.6 °C (mean  $\pm$  1 std. dev. of climate data from seven GCMs, same hereafter) in 2080 – 2099 (Figure S4). A/ is expected to decrease from 0.55 during 2000 – 2019 to 0.49  $\pm$  0.02 during 2080 – 2099 (Figure S5). By the end of the 21st century in the RCP45, only four ecoregions are projected to fall within the optimal climatic ranges for redcedar habitat, including Ozark Highlands (A/ = 0.84  $\pm$  0.07,  $T_{avg}$  = 18.3  $\pm$  0.7 °C), Central Irregular Plains (A/ = 0.79  $\pm$  0.06,  $T_{avg}$  =

 $17.1 \pm 0.8 \,^{\circ}C$ ), Western Corn Belt Plains (AI = 0.70  $\pm$  0.06,  $T_{avg}$  =  $15.2 \pm 0.8 \,^{\circ}C$ ), and Flint Hills (AI =  $0.68 \pm 0.06$ ,  $T_{avg}$  =

 $16.3\pm0.8$  °C). In the RCP85, the SGP states are projected to experience even higher temperature and drier climate conditions. The annual temperature for the study domain is expected to rise from 17.0 °C during 2000 – 2019 to 22.1  $\pm$  0.8 °C during 2080 – 2099, while AI is predicted to decrease from 0.55 during 2000 – 2019 to 0.44  $\pm$  0.03 during 2080 – 2099. Western Corn

Belt Plains is anticipated to be the only ecoregion that falls within the optimal ranges for AI and  $T_{avg}$ , simultaneously, by the end of the 21st century in the RCP85.

With the projected changes in future climate conditions, the regions with the optimal AI will shift eastward in the 21st century under both the RCP45 and RCP85 scenarios (Fig. 7). In the period from 2000 to 2019, the average longitude of the lower boundary of AI (AI = 0.6) is approximately 97.9 °W. Future climate projections indicate that in the four 20-year future periods under the RCP45, the average longitudes of the low AI boundary will shift to 97.4 °W, 97.2 °W, 97.2 °W, and 97.2 °W, respectively. Similarly, in the RCP85, the average longitudes of the lower AI boundary are projected to be around 97.5 °W, 97.1 °W, 96.8

°W, and 96.6 °W for the respective future periods. Overall, the optimal AI boundary will shift eastward by approximately 0.7° ( $\approx$  58 km) in the RCP45 and 1.3° ( $\approx$  108 km) in the RCP85 across the 21st century. This analysis focused on the spatial shift of the lower AI boundary rather than the upper boundary, which is projected to extend beyond the eastern side of the study domain.

Meanwhile, the region with the optimal annual temperature will move northward during the five 20-year periods of the 21st century in both the RCP45 and RCP85 scenarios (Fig. 8). In the contemporary period (2000 – 2019), the average latitude of the upper boundary of  $T_{avg}$  ( $T_{avg}$  = 18.6) is located at 31.4 °N. Under the RCP45, the average latitudes of the upper  $T_{avg}$  boundary will shift to 33.0 °N, 33.6 °N, 34.6 °N, and 35.0 °N, respectively, during the four 20-year future periods. In the RCP85, the average latitudes of the upper  $T_{avg}$  boundary will be at 32.8

°N, 35 °N, 36.2 °N, 38.0 °N, respectively. Overall, the optimal upper  $T_{avg}$  boundary is projected to have a northward shift by approximately 3.6° ( $\approx$  399 km) in the RCP45 and by 6.6° ( $\approx$  731 km) in the RCP85 throughout the 21st century. Noted that the analysis did not consider the shift in the lower boundary of the optimal  $T_{avg}$ , as it is projected to be beyond the northern side of the study domain.

# 3.3. Distribution probability in the contemporary period

During the contemporary period of 2000 – 2019, the average distribution probability of the study area was 0.23. The unsuitable, poorly suitable, moderately suitable, and highly suitable redcedar habitats accounted for 40.2 %, 31.6 %, 17.9 %, and 10.4 % of the study area, respectively, in the SGP states (Table 3). Among the 17 ecoregions in the study domain, the highest average distribution probability was observed in Ozark Highlands (0.8), Ouachita Mountains (0.8), and Arkansas Valley (0.79), which had percentages of highly suitable habitat of 97.0 %, 96.2 %, and 96.7 %, respectively. On the other hand, the ecoregions with the lowest average distribution probability were Southern Texas Plains (0.04), Edwards Plateau (0.08), Southwestern Tablelands (0.07), High Plains (0.04), and Chihuahuan Desert (0.04), with unsuitable habitat percentages of 94 %, 53.3 %, 61.6 %, 93.1 %, and 95.2 %,

24

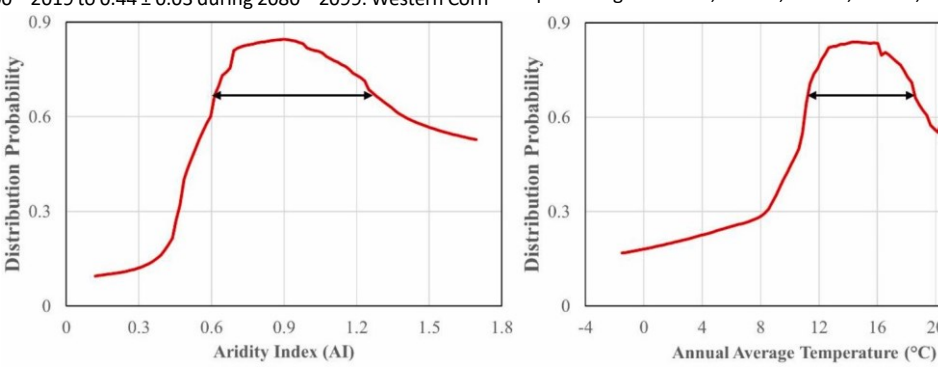


Fig. 6. Response curve illustrating the response of redcedar distribution probability to Aridity Index (A) and annual average temperature (B) in the ensemble model. The double-sided arrows highlight the optimal ranges for Aridity Index (between 0.6 and 1.25) and annual average temperature (between 11 °C and 18.6 °C) with a distribution probability greater than

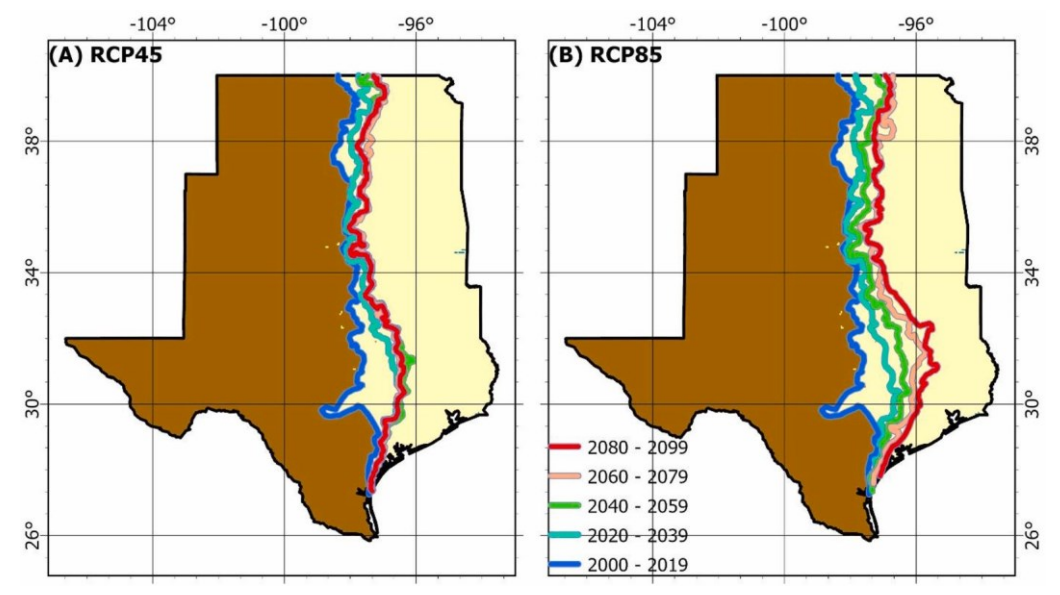


Fig. 7. The shift of the lower boundary of the optimal Aridity Index (AI = 0.6) in the RCP45 scenario (A) and RCP85 scenario (B) across the five 20-year periods of 2000 – 2019, 2020 – 2039, 2040 - 2059, 2060 - 2079, and 2080 - 2099. The background image represents the region within the optimal AI range (between 0.6 and 1.28, depicted in light yellow) for the period of 2000 - 2019.

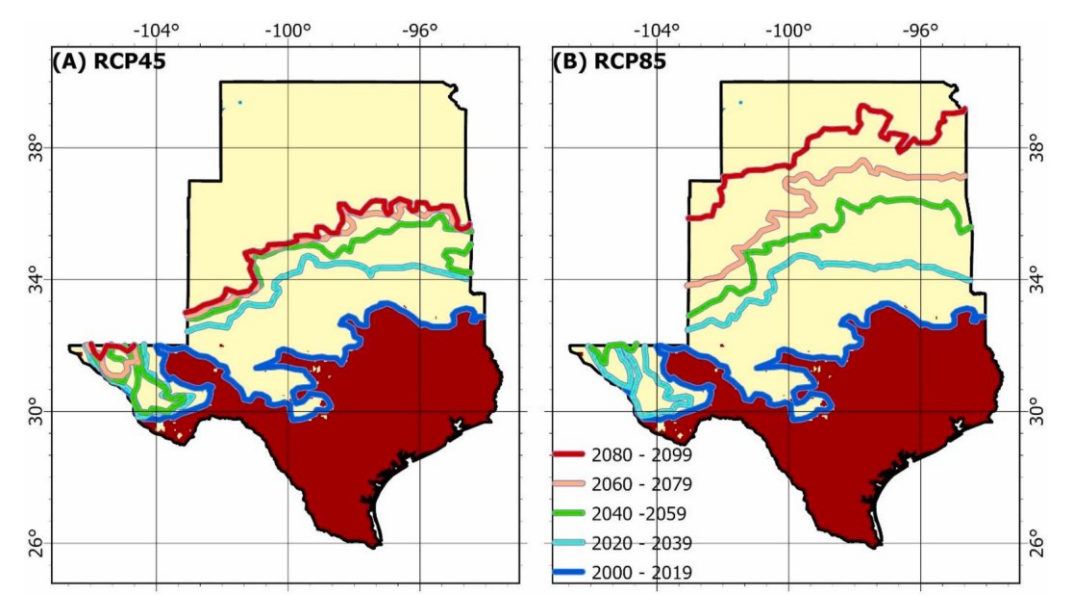


Fig. 8. The shift of the upper boundary of the optimal annual temperature ( $T_{ovg} = 18.6 \, ^{\circ}C$ ) during the five 20-year periods of 2000 – 2019, 2020 – 2039, 2040 – 2059, 2060 – 2079, and 2080 – 2099 in the RCP45 scenario (A) and the RCP85 scenario (B). The background image highlights the region within the optimal T<sub>ava</sub> range (between 11 °C and 18.6 °C, depicted in light yellow) during the period of 2000 – 2019. respectively.

Eastern redcedar showed a distinct west-to-east gradient of improving habitat quality in the study domain (Fig. 9). To the west of 101 °W, over 95 % of the land area was deemed unsuitable for the growth of eastern redcedar. However, as the longitude crosses 101 °W and moves towards the east, the distribution probability gradually increases (Fig. 9B and 9C). The most notable increase in distribution probability occurred within the longitude range between 100 °W and 97 °W. The highest distribution probability values were found within the longitude range of 97 °W and 94 °W, with particularly favorable conditions in Oklahoma.

# 3.4. Future changes in distribution probability

Distribution probability for eastern redcedar in the study domain is expected to have a continuous decline in the five 20-year periods under both the RCP45 and RCP85 scenarios (Fig. 10). Across the entire study domain, the average distribution probability is projected to decrease from 0.23 in the period of 2000 – 2019 to 0.16  $\pm$  0.01 in the RCP45 and to 0.12  $\pm$  0.01 in the RCP85 in the period of 2080 – 2099 (Table S4). The most significant decline in distribution probability is anticipated to occur in the longitudinal region between 98 °W and 95 °W. Within this area, the distribution probability is projected to decrease from 0.53 during 2000 - 2019 to 0.36 in the RCP45 and 0.25 in the RCP85 during 2080 - 2099 (Figure S6). By the end of the 21st century, the ecoregions with the highest distribution probability are predicted to be  $\mbox{\it Ozark}$ 

Across the 21st century, the extent and locations of the four suitability classes will undergo considerable changes in response to the declining

 Table 3

 Statistics of the average distribution probability and the percentages of four habitat suitability classes in the study domain and each individual ecoregion for the period of 2000 – 2019.

	Average Distribution Probability	Percentage of unsuitable (%)	Percentage of poorly suitable (%)	Percentage of moderately suitable (%)	Percentage of highly suitable (%)
Entire study domain	0.23	40.2	31.6	17.9	10.4
South Central Plains	0.57	0.0	12.5	54.5	33.0
Ozark Highlands	0.8	0.0	0.0	3.0	97.0
Ouachita Mountains	0.8	0.0	0.0	3.7	96.2
Central Irregular Plains	0.57	0.0	1.1	76.7	22.2
Arkansas Valley	0.79	0.0	0.0	3.3	96.7
Western Corn Belt Plains	0.47	0.0	16.1	80.2	3.7
Flint Hills	0.5	0.0	6.7	85.3	8.0
East Central Texas Plains	0.47	1.8	28.5	48.3	21.4
Western Gulf Coastal Plain	0.13	12.4	82.3	5.2	0.0
Texas Blackland Prairies	0.35	0.1	51.0	44.4	4.6
Cross Timbers	0.41	0.0	50.3	20.1	29.6
Central Great Plains	0.24	10.5	60.6	25.6	3.3
Southern Texas Plains	0.04	94.0	6.0	0.0	0.0
Edwards Plateau	0.08	53.3	46.4	0.3	0.0
Southwestern Tablelands	0.07	61.6	36.1	2.8	0.0
High Plains	0.04	93.1	6.9	0.0	0.0
Chihuahuan Desert	0.04	95.2	4.8	0	0

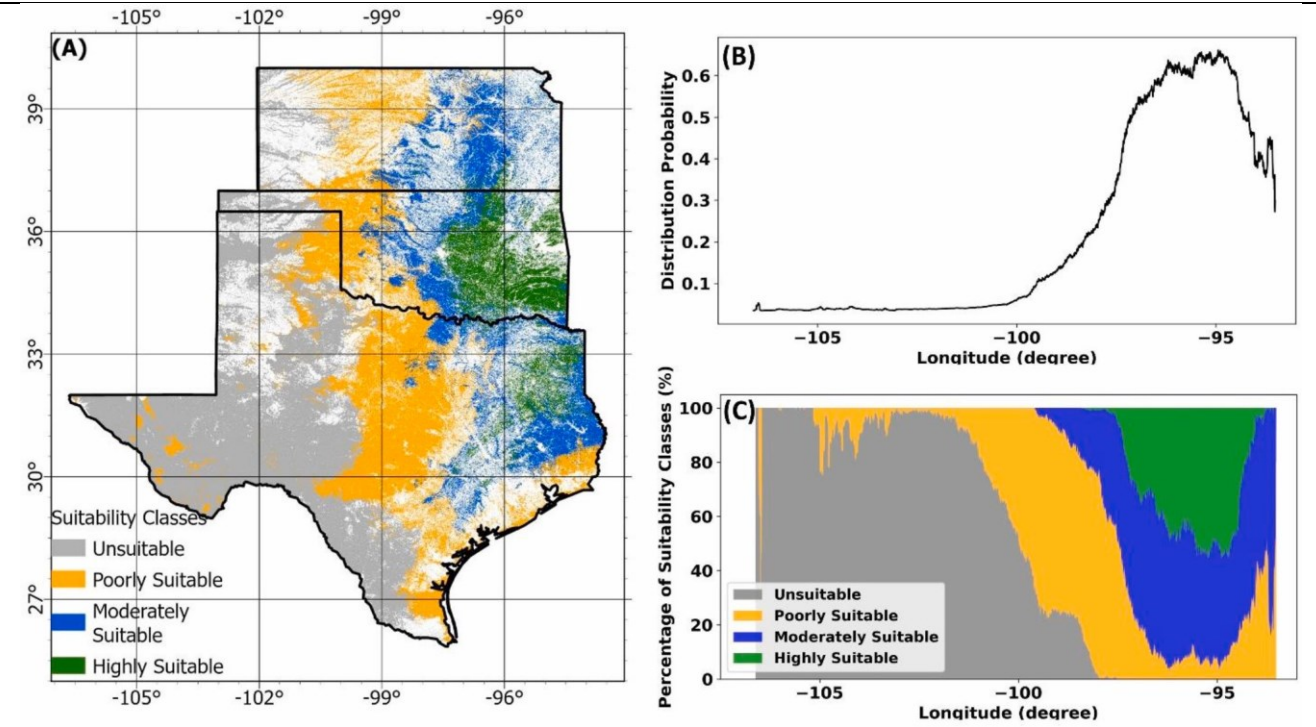
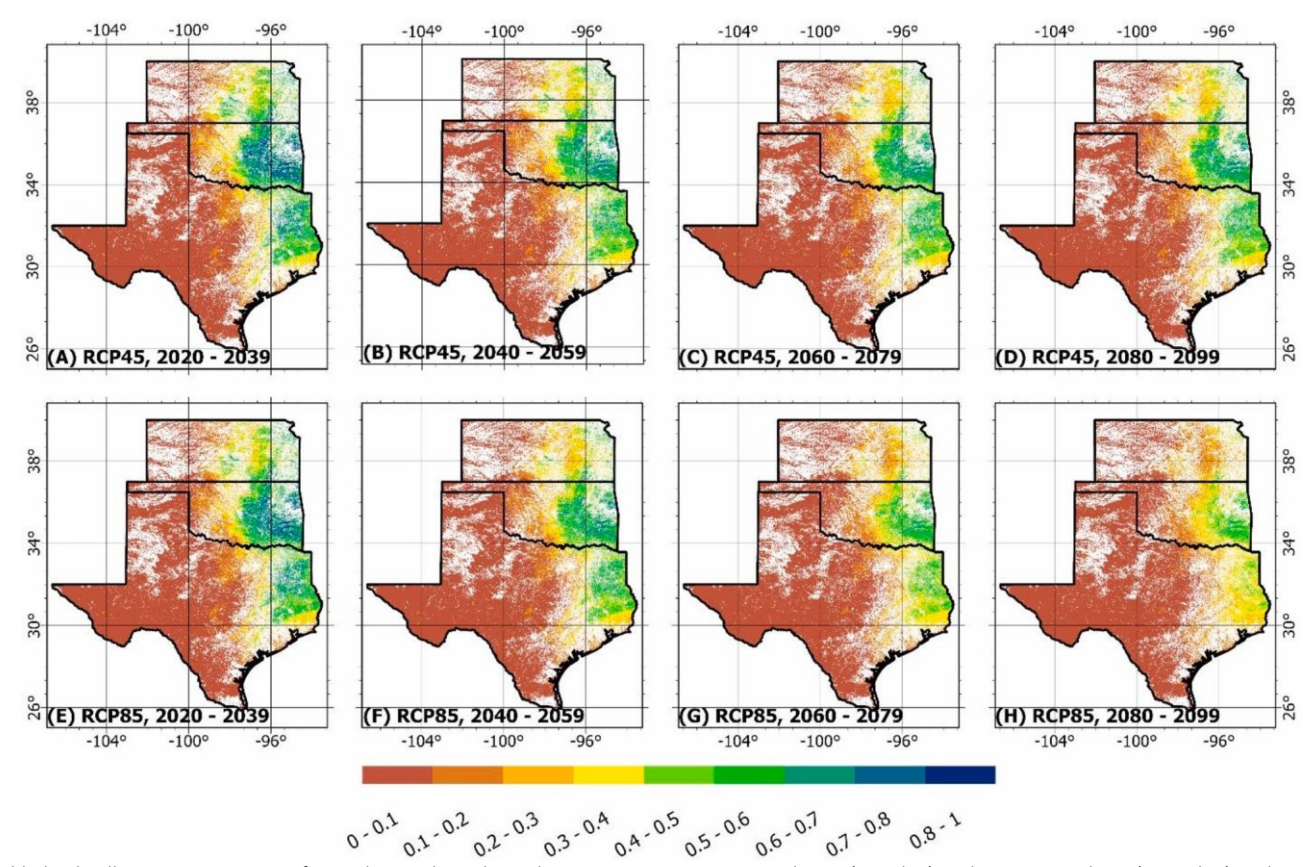


Fig. 9. Spatial pattern of eastern redcedar suitability classes over the period of 2000 – 2019 based on the simulated distribution probability from the ensemble model. (A) spatial pattern of four suitability classes, (B) latitudinal averages of distribution probability and their changes in the longitudinal direction, and (C) latitudinal average of the percentages of four suitability classes and their changes in the longitudinal direction.

Highlands (0.59  $\pm$  0.06 in the RCP45 and 0.48  $\pm$  0.03 in the RCP85), Ouachita Mountains (0.61  $\pm$  0.04 in the RCP45 and 0.49  $\pm$  0.03 in the RCP85), and Arkansas Valley (0.59  $\pm$  0.04 in the RCP45 and 0.46  $\pm$  0.04 in the RCP85).

distribution probability (Fig. 11). The proportion of study area categorized as unsuitable is projected to increase from 40.2% during

2000 - 2019 to  $48 \pm 1.8\%$  during 2080 - 2099 in the RCP45, and to  $54.2 \pm 2.3\%$  during 2080 - 2099 in the RCP85 (Fig. 12). While the total area of poorly



suitable land will not experience significant change throughout the century, the spatial centroid of the poorly suitable land will shift eastward by

approximately 0.6° ( $\approx$  49 km) in the RCP45 and 1.2° ( $\approx$  103 km) in the RCP85 over the course of the century. Since the

Fig. 10. Spatial pattern and temporal changes in the distribution probability of eastern redcedar over the four 20-year periods of 2020 – 2039, 2040 – 2059, 2060 – 2079, and 2080 – 2099 in the RCP45 (A, B, C, and D) and the RCP85 (E, F, G, and H) scenarios.

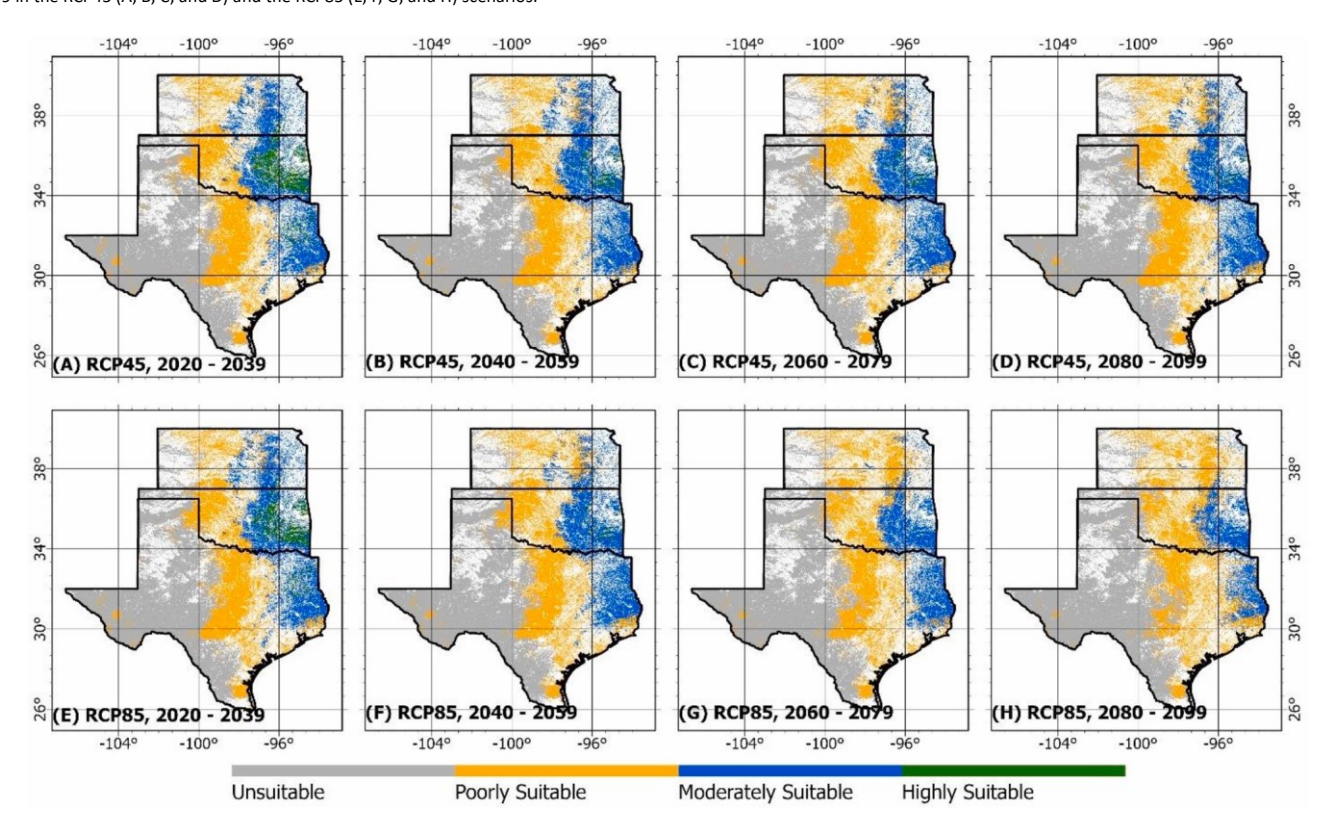


Fig. 11. Spatial pattern and temporal changes in the four suitability classes for eastern redcedar growth during the periods of 2020 – 2039, 2040 – 2059, 2060 – 2079, and 2080 – 2099 under the RCP45 (A, B, C, and D) and the RCP85 (E, F, G, and H) scenarios.

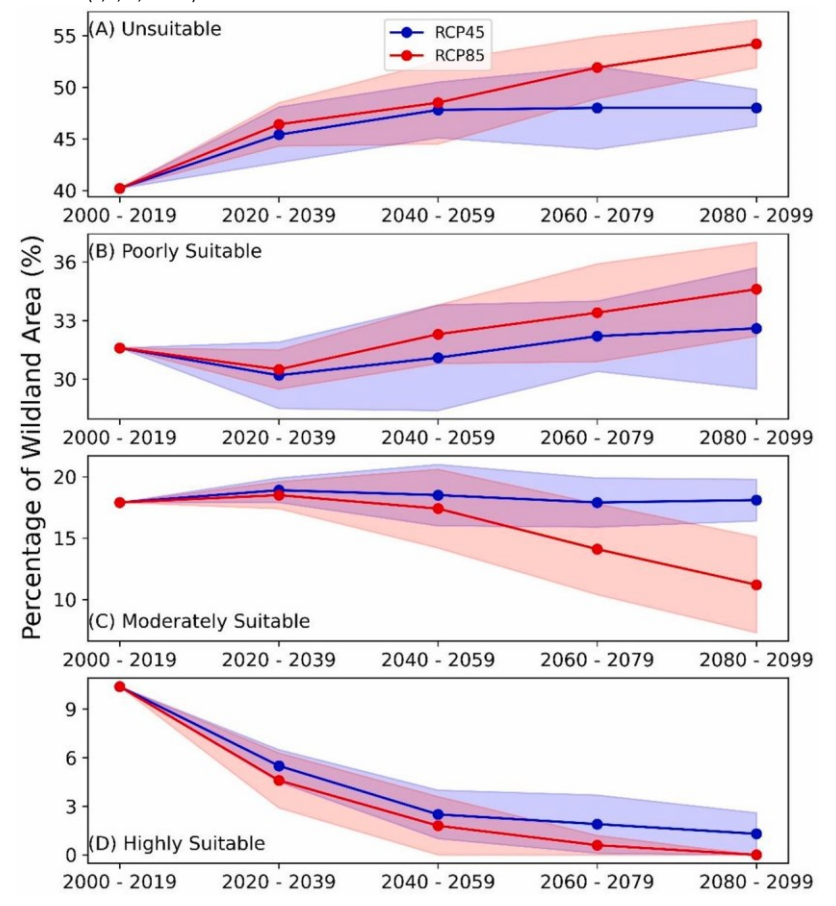


Fig. 12. Temporal changes in the percentages of the four habitat suitability classes, namely, (A) Unsuitable, (B) Poorly Suitable, (C) Moderately Suitable, and (D) Highly Suitable, in the study domain over the course of the five 20-year periods in the 21st century.

poorly suitable class predominantly distributes within the study domain throughout the entire study period, it is used as a proxy to represent the spatial shift of all habitat suitability classes. Moderately suitable land area will diverge between the RCP45 and RCP85 scenarios. In the RCP45, the percentage of the moderately suitable land area is expected to have a slight increase from 17.9 % to  $18.1\pm1.7\%$  by the end of the 21st century. Conversely, in the RCP85, it will decrease significantly from 17.9% to  $11.2\pm3.9\%$  (Fig. 10). For the highly suitable class, there will be a similar declining pattern in both the RCP45 and the RCP85, with the area decreasing from 10.4% during 2000 – 2019 to  $1.3\pm1.3\%$  in the RCP45 and  $0\pm0\%$  in the RCP85 by the end of the 21st century.

By the end of the 21st century in both the RCP45 and RCP85 scenarios, over 99 % of the land area that was classified as unsuitable during 2000-2019 will remain unsuitable for redcedar to grow (Table 4). However, a significant portion of the land area initially classified as suitable during 2000-2019 will experience a degradation in suitability classes. In the RCP45, 22.4 % of poorly suitable land area

#### Table 4

during 2000 – 2019 will transition into unsuitable habitats by the end of the 21st century. In the RCP85, this percentage will be 41.4 %. Regarding moderately suitable class, 50 % of the area will transition into poorly suitable class in the RCP45, while a higher proportion of 84.1 % will become poorly suitable in the RCP85. Additionally, in the RCP45, 92.5 % of highly suitable habitat will transition into either moderately suitable or poorly suitable classes by the end of the 21st century. In the RCP85 scenario, all highly suitable habitats will transition into either moderately suitable or poorly suitable classes.

3.5. Dissimilarity of environmental variables between training samples and future projection

Fig. 13 illustrates the average MESS derived from future projections driven by climate datasets from 7 GCMs for four 20-year future periods under the RCP45 and RCP85 scenarios. Negative MES values suggest a significant level of uncertainty, particularly in southern Texas,

		Un- suitable	Poorly Suitable	Moderately Suitable	Highly Suitable	Un- suitable	Poorly Suitable	Moderately Suitable	Highly Suitable
2000 -	Unsuitable	99.5 %	0.5 %	_	_	99.7 %	0.3 %	_	_
2019	<b>Poorly Suitable</b>	22.4 %	76.5 %	1 %	_	41.4 %	58.5 %	0.4 %	-
	<b>Moderately Suitable</b>	_	50 %	50 %	_	_	84.1 %	15.9 %	_

 Highly Suitable
 1.4%
 91.1%
 7.5%
 23%
 77%
 0%

RCP45, 2080 - 2099 RCP85, 2080 - 2099

The transition of habitat suitability classes from the period of 2000 – 2019 to the period of 2080 – 2099 under the RCP45 and the RCP85 scenarios. The percentages in this table indicate the proportion of each suitability class in 2000 – 2019 that transitions to the four suitability classes by the end of this century.

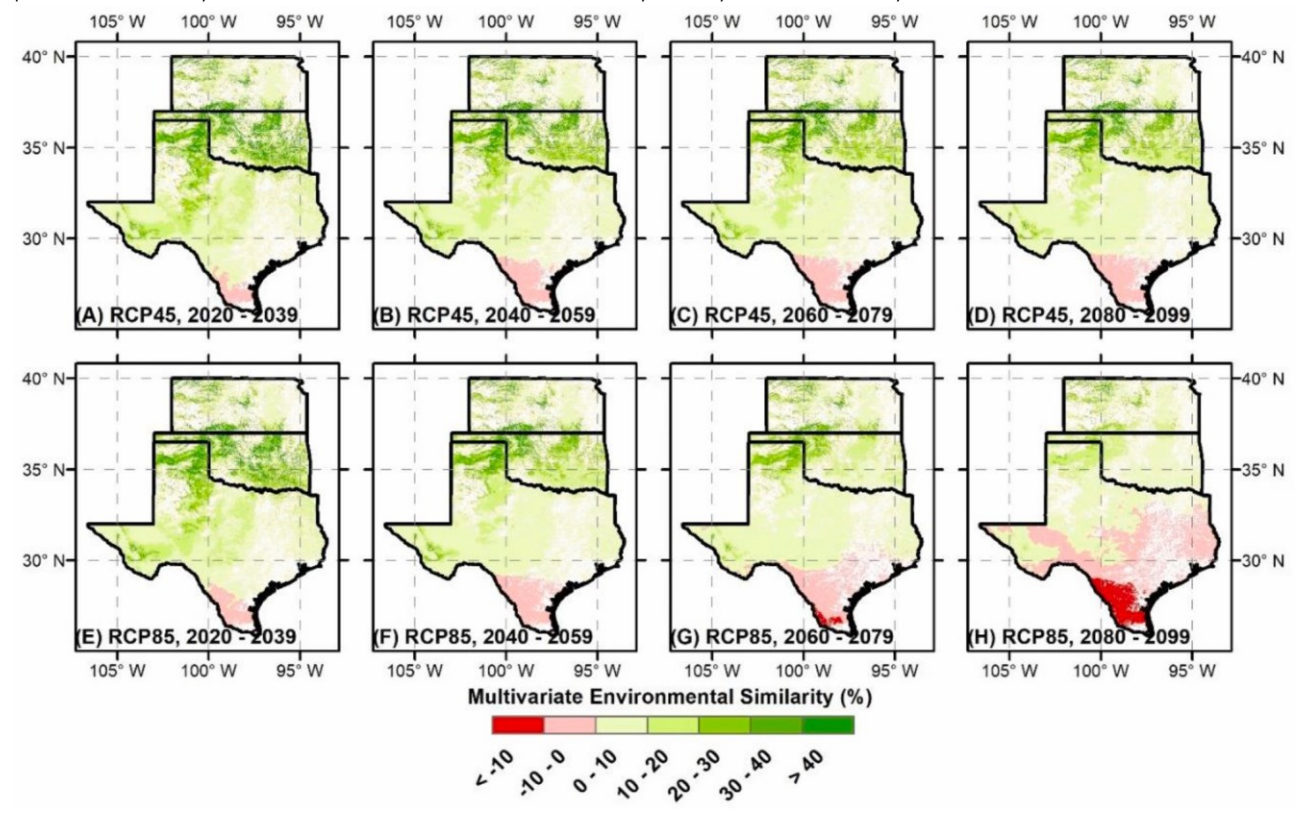


Fig. 13. Multivariate Environmental Similarity Surface (MESS) for the projections in four 20-year future periods of 2020 – 2039, 2040 – 2059, 2060 – 2079, and 2080 – 2099. The simulations are conducted under two climate scenarios: RCP45 (A, B, C, and D) and RCP85 (E, F, G, and H). The MESS maps illustrate the average value of Multivariate Environmental Similarity (MES) driven by climate data from seven General Circulation models.

highlighting notable discrepancies between the training dataset and future climate conditions in that region. Furthermore, the spatial extent of areas with negative MES values is expected to expand as time progresses. In the last 20-year period of the 21st century, the proportions of areas with negative MES values are projected to be 8.7% under the RCP45 and 34.5% in the RCP85, respectively.

 $T_{ovg}$  was identified to be the Most Dissimilar Variable (MDV) in the future projections for most of the study area with negative MES value (Figure S7). This is not surprising, given the projected rapid increase in annual temperature in the study area, particularly in the RCP85 scenario (Figure S4). This temperature rise is expected to push the southern Texas region beyond the temperature range in the training dataset, contributing to the dissimilarity between the reference data and the future environmental conditions. It is worth noting that AI will not be the MDV, except for a small area in western Texas under the RCP85 during the period of 2080 – 2099 (Figure S7H). Considering that AI is the most important variable in the SDMs (Table 2) and future AI values are expected to largely fall within the range of the training data, the projected future distribution probability is anticipated to have high reliability.

#### 4. Discussion

## 4.1. Environmental factors influencing habitat suitability

The SDMs in this study incorporated three types of environmental factors: climate, soil properties, and topography. Among these factors, climate conditions, particularly the long-term average aridity, were the most

significant variable in shaping the spatial pattern of eastern redcedar habitat suitability (Table 2). This finding is consistent with previous research showing the crucial role of precipitation regimes in determining the growth and extent of woody plants (Archer et al., 2017). Therefore, future changes in eastern redcedar habitat suitability in the SGP will be primarily driven by the projected drying trend. Our findings indicate that the optimal aridity range for redcedar habitat in the 21st century will shift eastward by approximately  $0.7^{\circ}$  ( $\approx$  58 km) under the RCP45 and by approximately  $1.3^{\circ}$  ( $\approx$  108 km) under the RCP85 (Fig. 7). Consequently, the spatial centroid of the suitable land area will also shift eastward by  $0.6^{\circ}$  ( $\approx$  49 km) under the RCP45 and by  $1.2^{\circ}$  ( $\approx$  103 km) under the RCP85 (Fig. 11). These shifts are expected to significantly reduce the overall area of suitable land for eastern redcedar growth in the mixed prairie and the west of the SGP states.

Fire regimes and grazing are potential factors influencing the distribution of eastern redcedar in the SGP (Fuhlendorf et al., 2008). However, due to the lack of accurate future projections of wildfire regimes, the extent of prescribed burning, and livestock density, these factors were not explicitly incorporated into the development of the SDMs and future projections in this study. Wildfire regimes are strongly correlated with regional climate conditions (Abatzoglou and Williams, 2016; Westerling et al., 2003; Yang et al., 2015). Therefore, by incorporating climate factors (i.e., AI and  $T_{ovg}$ ) into the SDMs, some implicit information related to future changes in wildfire regimes had been indirectly considered in these simulations.

#### 4.2. Implications for land management and ecosystem composition

The negative impacts of eastern redcedar encroachment on ecosystem services and agricultural production have been widely recognized by stakeholders. In response, government agencies and organizations have implemented various incentive programs to support the reduction of eastern redcedar in the SGP (Fogarty et al., 2021). For example, USDA NRCS allocated \$5.5 million to \$7 million each year through the Environmental Quality Incentive Program (EQIP) to assist Oklahoma landowners in addressing natural resource concerns and improving environmental quality. A large fraction of this fund has been dedicated to supporting the removal of eastern redcedar from rangelands. Our simulation results indicate that future climate change will decrease redcedar habitat suitability and limit its encroachment in the western region of the SGP states. Therefore, based on this information, we cautiously suggest that stakeholders prioritize the allocation of redcedar removal resources and efforts in the humid and semi-humid ecoregions in the eastern portion of the SGP states.

Prescribed burning has been used by landowners in the SGP to improve forage quality and clear hazardous fuels, including redcedar (Twidwell et al., 2013b). The implementation of pyric herbivory, which involves the synergistic integration of livestock grazing and patch burning, is an effective option for controlling eastern redcedar encroachment (Fuhlendorf et al., 2017; Wilcox et al., 2022). This approach creates a shifting mosaic of landscape patches with varying prescribed burning schedules and post-fire recovery. Pyric herbivory is a cost-effective management strategy and offers numerous benefits, including maintaining open grasslands (Twidwell et al., 2013b), enhancing forage quality and production (Boughton et al., 2022), reducing woody plants (Capozzelli et al., 2020), and creating breeding habitats for grassland birds (Augustine and Derner, 2015). Furthermore, the development of industries that utilize eastern redcedar, such as the manufacturing of mulch, particleboard, and biofuel, can make a significant contribution to the local and regional economy (Kaur et al., 2020). This highlights the potential of effective management strategies for eastern redcedar to not only address environmental and agricultural challenges but also provide economic opportunities and promote sustainable utilization of this resource.

Our simulation results revealed that with climate warming and drying in the future, a significant portion of currently suitable lands in the western and central regions of the SGP states, particularly under the RCP85 scenario, will become unsuitable for eastern redcedar. This change is attributable to the increased occurrence of droughts and heatwaves, which would lead to higher mortality rates among eastern redcedar and other tree species (Allen et al., 2010). The eastern part of the SGP states will also experience a reduction in habitat suitability, with the suitability class transitioning from highly suitable to moderately suitable. This means that redcedar trees are still expected to have higher chances of survival and growth in the east. Currently, the dominant tree species in the eastern ecoregions are oaks, such as Quercus stellata and Q. marilandica (Hoff et al., 2018a). Eastern redcedar encroachment into these oak-dominated forests began in the 1950s and has not yet reached its full potential. Given that eastern redcedar has greater drought tolerance and lower mortality rates related to drought compared to oak species (Gu et al., 2015; Torquato et al., 2020b), it is likely that redcedar trees will continue to encroach into deciduous forests under future climate conditions. If unchecked, this could result in the gradual replacement of oakdominated forests by redcedar trees.

# 4.3. Employed strategies to mitigate uncertainties

To reduce uncertainties in future simulations, several strategies were implemented in this study. During the model training and simulation processes, we obtained USDA FIA eastern redcedar samples and implemented simulations in eight states, which covered a larger spatial extent than the three SGP states. This approach ensured that the range of AI in the training dataset encompassed a wide spectrum and reduced the chances of future AI to exceed the range. Recognizing the divergence in future climate projections

among different GCMs (Sillmann et al., 2013), this study followed an approach in J. Yang et al. (2023) and reported the average and standard deviation of simulation results driven by seven climate datasets from different GCMs. This strategy accounted for the variations in the projected future climate conditions by GCMs and increased confidence in the interpretation of projected patterns of future redcedar distribution probability. Additionally, every single SDM has limitations in its spatial projection (Lissovsky and Dudov, 2021). To mitigate this uncertainty, we employed an ensemble approach based on the results of seven SDMs to reduce the biases in these individual models, resulting in more robust estimates of future habitat suitability (Shabani et al., 2016).

## 4.4. Caveats and future research needs

Currently, redcedar and honey mesquite (Prosopis glandulosa) coexist within the same ecological niche in the western region of the study domain. Honey mesquite, known for its greater drought tolerance, thrives in these arid environment conditions. As the climate continues to become drier, it is expected that intensified competition between redcedar and mesquite will occur, resulting in significant changes in their dynamics and contributing to the confinement of redcedar to the western boundary. The eastern region of our study domain has optimal conditions for the growth of eastern redcedar trees. However, their distribution in this area is limited by competition from faster growing mesic trees (Lawson, 1990). Therefore, to obtain a more accurate projection of redcedar future distribution, it would be highly beneficial to use an approach that incorporates not only the abiotic attributes but also species-specific competition in future endeavors. To achieve this, future studies could consider forest landscape models, such as LANDIS-II (Scheller et al., 2007), to simulate the changing distribution of eastern redcedar by simulating the competition between woody plant species. Additionally, we acknowledge that in southern Texas, the future annual temperature will exceed the upper boundary of the temperature range in model training samples (Fig. 13). As a result, model results for this region carried higher uncertainty and caution should be exercised when making interpretations in this region. Moreover, SDMs in this study did not consider the relationship between eastern redcedar and other biotic components, such as pests and diseases, which can lead to uncertainties in the projected distribution probability.

#### 5. Conclusion

The encroachment of eastern redcedar poses a significant threat to ecosystem services in the SGP forests and grasslands. In this study, we utilized an ensemble approach of seven SDMs to project the spatiotemporal patterns of eastern redcedar distribution probability under future climate conditions. The simulation results indicate that throughout the 21st century, the suitable habitat for eastern redcedar will shift eastward by  $0.6^{\circ}$  ( $\approx 49$  km) in the RCP45 and by  $1.2^{\circ}$  ( $\approx 103$  km) in the RCP85. These changes in habitat suitability will render most of the western region of the SGP states unsuitable for redcedar growth. However, although redcedar habitat suitability will decrease in the eastern regions of the SGP as well, it is still possible for eastern redcedar to grow and thrive. Based on these results, we suggest that stakeholders prioritize the allocation of redcedar removal resources and efforts in the humid and semi-humid ecoregions in the eastern portion of the SGP states, particularly in the context of the RCP85 scenario.

#### **Declaration of Competing Interest**

The authors declare that they have no known competing financial interests or personal relationships that could have appeared to influence the work reported in this paper.

#### Acknowledgements

This work was supported by the Oklahoma NSF EPSCoR S3OK project (award number: OIA-1946093), S3OK project Research Seed Grant, USDA McIntire-Stennis Grant (OKL03249, OKL03151, and OKL03152), USGS South Central Climate Adaptation Science Center grant, and Joint Fire Science Program grant. This work was partially supported by R.W.'s Sarkeys Distinguished Professorship. The Authors declare that there are no conflicts of interests.

## Supplementary materials

Supplementary material associated with this article can be found, in the online version, at doi:10.1016/j.agrformet.2023.109836.

#### References

- Abatzoglou, J.T., 2013. Development of gridded surface meteorological data for ecological applications and modelling. Int. J. Climatol. 33, 121–131. https://doi.org/10.1002/joc.3413.
- Abatzoglou, J.T., Brown, T.J., 2012. A comparison of statistical downscaling methods suited for wildfire applications. Int. J. Climatol. 32, 772–780. https://doi.org/10.1002/joc.2312.
- Abatzoglou, J.T., Williams, A.P., 2016. Impact of anthropogenic climate change on wildfire across western US forests. Proc. Natl. Acad. Sci. 113, 11770–11775. https://doi.org/10.1073/pnas.1607171113.
- Allen, C.D., Macalady, A.K., Chenchouni, H., Bachelet, D., McDowell, N., Vennetier, M., Kitzberger, T., Rigling, A., Breshears, D.D., Hogg, E.H.(Ted), Gonzalez, P., Fensham, R., Zhang, Z., Castro, J., Demidova, N., Lim, J.H., Allard, G., Running, S. W., Semerci, A., Cobb, N., 2010. A global overview of drought and heat-induced tree mortality reveals emerging climate change risks for forests. Forest Ecology and Management, Adaptation of Forests and Forest Management to Changing Climate 259, 660–684. https://doi.org/10.1016/j.foreco.2009.09.001.
- Anadon, J.D., Sala, O.E., Turner, B.L., Bennett, E.M., 2014. Effect of woody-plant 'encroachment on livestock production in North and South America. Proc. Natl. Acad. Sci. 111, 12948– 12953. https://doi.org/10.1073/pnas.1320585111.
- Archer, S., Andersen, E., Predick, K., Schwinning, S., Steidl, R., Woods, S., 2017. Chapter 2 Woody Plant Encroachment: Causes and Consequences. Rangeland Systems. Springer. pp. 25–84.
- Archer, S.R., Predick, K.I., 2014. An ecosystem services perspective on brush management: research priorities for competing land-use objectives. J. Ecol. 102, 1394–1407. https://doi.org/10.1111/1365-2745.12314.
- Augustine, D.J., Derner, J.D., 2015. Patch-burn grazing management, vegetation heterogeneity, and avian responses in a semi-arid grassland. J. Wildl. Manage. 79, 927–936. https://doi.org/10.1002/jwmg.909.
- Barger, N.N., Archer, S.R., Campbell, J.L., Huang, C., Morton, J.A., Knapp, A.K., 2011. Woody plant proliferation in North American drylands: A synthesis of impacts on ecosystem carbon balance. J. Geophys. Res. 116 https://doi.org/10.1029/2010JG001506.
- Bennion, L.D., 2023. Mechanisms of Eastern Redcedar Encroachment At Multiple Spatial Scales. Kent State University.
- Bennion, L.D., Ward, D., 2022. Plant—soil feedback from eastern redcedar (Juniperus virginiana) inhibits the growth of grasses in encroaching range. Nat. Ecol. Evol. 12, e9400. https://doi.org/10.1002/ece3.9400.
- Boughton, E.H., Gomez-Casanovas, N., Swain, H., Bernacchi, C., Boughton, R.K., Brinsko, K., Li, H., Rivero, A., DeLucia, E.H., Sparks, J., 2022. Patch-Burn Grazing Impacts Forage Resources in Subtropical Humid Grazing Lands. Rangeland Ecology & Management 84, 10–21. https://doi.org/10.1016/j.rama.2022.05.004.
- Box, T.W., 1967. Range Deterioration in West Texas, Southwest Hist, O. 71, 37–45.
- Breshears, D.D., Cobb, N.S., Rich, P.M., Price, K.P., Allen, C.D., Balice, R.G., Romme, W. H., Kastens, J.H., Floyd, M.L., Belnap, J., Anderson, J.J., Myers, O.B., Meyer, C.W., 2005. Regional vegetation die-off in response to global-change-type drought. Proc.
  - Natl. Acad. Sci. 102, 15144–15148. https://doi.org/10.1073/pnas.0505734102.
- Capozzelli, J.F., Miller, J.R., Debinski, D.M., Schacht, W.H., 2020. Restoring the fire–grazing interaction promotes tree–grass coexistence by controlling woody encroachment. Ecosphere 11, e02993. https://doi.org/10.1002/ecs2.2993.
- Dormann, C.F., Elith, J., Bacher, S., Buchmann, C., Carl, G., Carre, G., Marquí 'ez, J.R.G., Gruber, B., Lafourcade, B., Leitao, P.J., Münkemüller, T., McClean, C., Osborne, P.E., "Reineking, B., Schroder, B., Skidmore, A.K., Zurell, D., Lautenbach, S., 2013. "Collinearity: a review of methods to deal with it and a simulation study evaluating their performance. Ecography 36, 27–46. https://doi.org/10.1111/j.1600-0587.2012.07348.x.
- Elith, J., Kearney, M., Phillips, S., 2010. The art of modelling range-shifting species. Methods Ecol. Evol. 1, 330–342. https://doi.org/10.1111/j.2041-210X.2010.00036. x.
- Elith, J., Phillips, S.J., Hastie, T., Dudík, M., Chee, Y.E., Yates, C.J., 2011. A statistical explanation of MaxEnt for ecologists. Divers. Distrib. 17, 43–57. https://doi.org/10.1111/j.1472-4642.2010.00775.x
- Evans, J.S., Murphy, M.A., Holden, Z.A., Cushman, S.A., 2011. Modeling Species Distribution and Change Using Random Forest. In: Drew, C.A., Wiersma, Y.F., Huettmann, F. (Eds.), Predictive Species and Habitat Modeling in Landscape Ecology: Concepts and Applications. Springer, New York, NY, pp. 139–159. https://doi.org/10.1007/978-1-4419-7390-0\_8.

- Feng, X., Park, D.S., Liang, Y., Pandey, R., Papes, M., 2019. Collinearity in ecological niche modeling: Confusions and challenges. Nat. Ecol. Evol. 9, 10365–10376. https://doi.org/10.1002/ece3.5555.
- Filippelli, S.K., Vogeler, J.C., Falkowski, M.J., Meneguzzo, D.M., 2020. Monitoring conifer cover: Leaf-off lidar and image-based tracking of eastern redcedar encroachment in central Nebraska. Remote Sens. Environ. 248, 111961 https://doi. org/10.1016/j.rse.2020.111961.
- Fogarty, D.T., de Vries, C., Bielski, C., Twidwell, D., 2021. Rapid Re-encroachment by Juniperus virginiana After a Single Restoration Treatment. Rangeland Ecology & Management, Great Plains 78, 112–116. https://doi.org/10.1016/j. rama.2021.06.002.
- Franklin, J., 2010. Mapping Species distributions: Spatial Inference and Prediction. Cambridge University Press.
- Fuhlendorf, S.D., Archer, S.A., Smeins, F., Engle, D.M., Taylor, C.A., 2008. The Combined Influence of Grazing, Fire, and Herbaceous Productivity on Tree—Grass Interactions. In: Van Auken, O.W. (Ed.), Western North American Juniperus Communities: A Dynamic Vegetation Type, Ecological Studies. Springer, New York, NY, pp. 219–238. https://doi.org/10.1007/978-0-387-34003-6 12.
- Fuhlendorf, S.D., Fynn, R.W., McGranahan, D.A., Twidwell, D., 2017. Heterogeneity as the basis for rangeland management. Rangeland Systems: Processes, Management and Challenges 169–196.
- Gu, L., Pallardy, S.G., Hosman, K.P., Sun, Y., 2015. Drought-influenced mortality of tree species with different predawn leaf water dynamics in a decade-long study of a central US forest. Biogeosciences 12, 2831–2845. https://doi.org/10.5194/bg-12-2831-2015.
- Guillera-Arroita, G., Lahoz-Monfort, J.J., Elith, J., Gordon, A., Kujala, H., Lentini, P.E., McCarthy, M.A., Tingley, R., Wintle, B.A., 2015. Is my species distribution model fit for purpose? Matching data and models to applications. Global Ecol. Biogeogr. 24, 276–292. https://doi.org/10.1111/geb.12268.
- Guisan, A., Edwards, T.C., Hastie, T., 2002. Generalized linear and generalized additive models in studies of species distributions: setting the scene. Ecol. Modell. 157, 89–100. https://doi.org/10.1016/S0304-3800(02)00204-1.
- Hoff, D.L., Will, R.E., Zou, C.B., Lillie, N.D., 2018a. Encroachment Dynamics of Juniperus virginiana L. and Mesic Hardwood Species into Cross Timbers Forests of North- Central Oklahoma, USA. Forests 9, 75. https://doi.org/10.3390/f9020075.
- Hoff, D.L., Will, R.E., Zou, C.B., Weir, J.R., Gregory, M.S., Lillie, N.D., 2018b. Estimating increased fuel loading within the Cross Timbers forest matrix of Oklahoma, USA due to an encroaching conifer, Juniperus virginiana, using leaf-off satellite imagery. Forest Ecol. Manag. 409, 215– 224. https://doi.org/10.1016/j.foreco.2017.11.003.
- Homer, C.H., Fry, J.A., Barnes, C.A., 2012. The national land cover database. US Geological Survey Fact Sheet 3020. 1–4.
- Huxman, T.E., Wilcox, B.P., Breshears, D.D., Scott, R.L., Snyder, K.A., Small, E.E., Hultine, K., Pockman, W.T., Jackson, R.B., 2005. Ecohydrological Implications of Woody Plant Encroachment. Ecology 86, 308–319. https://doi.org/10.1890/03-0583.
- Kaur, R., Joshi, O., Will, R.E., Murray, B.D., 2020. Sustainable management of unused eastern redcedar: An integrated spatial and economic analysis approach. Resour. Conserv. Recycl. 158, 104806 https://doi.org/10.1016/j.resconrec.2020.104806.
- Kishawi, Y., Mittelstet, A.R., Gilmore, T.E., Twidwell, D., Roy, T., Shrestha, N., 2023. Impact of Eastern Redcedar encroachment on water resources in the Nebraska Sandhills. Sci. Total Environ. 858, 159696 https://doi.org/10.1016/j. scitotenv.2022.159696.
- Kunkel, K.E., 2022. State Climate Summaries for the United States 2022. NOAA Technical Report NESDIS 150. NOAA NESDIS.
- Lawson, E.R., 1990. Juniperus virginiana L. eastern redcedar. Silvics of North America 1, 131–140.
- Lissovsky, A.A., Dudov, S.V., 2021. Species-Distribution Modeling: Advantages and Limitations of Its Application. 2. MaxEnt. Biol. Bull. Rev. 11, 265–275. https://doi.org/10.1134/S2079086421030087.
- Loss, S.R., Noden, B.H., Fuhlendorf, S.D., 2022. Woody plant encroachment and the ecology of vector-borne diseases. J. Appl. Ecol. 59, 420–430. https://doi.org/10.1111/1365-2664.14083
- Mainali, K.P., Warren, D.L., Dhileepan, K., McConnachie, A., Strathie, L., Hassan, G., Karki, D., Shrestha, B.B., Parmesan, C., 2015. Projecting future expansion of invasive species: comparing and improving methodologies for species distribution modeling. Global Change Biol. 21, 4464–4480. https://doi.org/10.1111/gcb.13038.
- Meneguzzo, D.M., Liknes, G.C., 2015. Status and Trends of Eastern Redcedar (Juniperus virginiana) in the Central United States: Analyses and Observations Based on Forest Inventory and Analysis Data. J. Forest. 113, 325–334. https://doi.org/10.5849/jof.14-093.
- Merow, C., Smith, M.J., Silander Jr, J.A., 2013. A practical guide to MaxEnt for modeling species' distributions: what it does, and why inputs and settings matter. Ecography 36, 1058–1069. https://doi.org/10.1111/j.1600-0587.2013.07872.x.
- Middleton, N., Thomas, D., 1997. World atlas of desertification.. ed. 2. Arnold, Hodder Headline, PLC.
- Miller, J., 2010. Species Distribution Modeling. Geography Compass 4, 490–509. https://doi.org/10.1111/i.1749-8198.2010.00351.x.
- Modala, N.R., Ale, S., Goldberg, D.W., Olivares, M., Munster, C.L., Rajan, N., Feagin, R. A., 2017. Climate change projections for the Texas High Plains and Rolling Plains. Theor. Appl. Climatol. 129, 263–280. https://doi.org/10.1007/s00704-016-1773-2.
- Phillips, S.J., 2005. A brief tutorial on Maxent. AT&T Research 190, 231–259.
- Phillips, S.J., Dudík, M., 2008. Modeling of species distributions with Maxent: new extensions and a comprehensive evaluation. Ecography 31, 161–175. https://doi. org/10.1111/j.0906-7590.2008.5203.x.
- Phillips, S.J., Dudík, M., Elith, J., Graham, C.H., Lehmann, A., Leathwick, J., Ferrier, S., 2009. Sample selection bias and presence-only distribution models: implications for background and pseudo-absence data. Ecol. Appl. 19, 181–197. https://doi.org/10.1890/07-2153.1.

- Poggio, L., de Sousa, L.M., Batjes, N.H., Heuvelink, G.B.M., Kempen, B., Ribeiro, E., Rossiter, D., 2021. SoilGrids 2.0: producing soil information for the globe with quantified spatial uncertainty. SOIL 7, 217–240. https://doi.org/10.5194/soil-7-217-2021.
- Polce, C., Garratt, M.P., Termansen, M., Ramirez-Villegas, J., Challinor, A.J., Lappage, M. G., Boatman, N.D., Crowe, A., Endalew, A.M., Potts, S.G., Somerwill, K.E., Biesmeijer, J.C., 2014. Climate-driven spatial mismatches between British orchards and their pollinators: increased risks of pollination deficits. Global Change Biol. 20, 2815–2828. https://doi.org/10.1111/gcb.12577.
- Priestley, C.H.B., Taylor, R.J., 1972. On the assessment of surface heat flux and evaporation using large-scale parameters. Mon. Weather Rev. 100, 81–92.
- Pyne, S.J., 2017. The Great Plains: a Fire Survey. University of Arizona Press.
- Pyne, S.J., 1984. Introduction to wildland fire. Fire management in the United States Introduction to wildland fire. Fire Management in the United States.
- Qiao, L., Zou, C.B., Stebler, E., Will, R.E., 2017. Woody plant encroachment reduces annual runoff and shifts runoff mechanisms in the tallgrass prairie, USA. Water Resour. Res. 53, 4838–4849. https://doi.org/10.1002/2016WR019951.
- Radosavljevic, A., Anderson, R.P., 2014. Making better Maxent models of species distributions: complexity, overfitting and evaluation. J. Biogeogr. 41, 629–643. https://doi.org/10.1111/jibi.12227.
- Remya, K., Ramachandran, A., Jayakumar, S., 2015. Predicting the current and future suitable habitat distribution of Myristica dactyloides Gaertn. using MaxEnt model in the Eastern Ghats, India. Ecological Engineering 82, 184–188. https://doi.org/ 10.1016/j.ecoleng.2015.04.053.
- Saintilan, N., Rogers, K., 2015. Woody plant encroachment of grasslands: a comparison of terrestrial and wetland settings. New Phytol. 205, 1062–1070. https://doi.org/ 10.1111/nph.13147.
- Sankaran, M., Hanan, N.P., Scholes, R.J., Ratnam, J., Augustine, D.J., Cade, B.S., Gignoux, J., Higgins, S.I., Le Roux, X., Ludwig, F., Ardo, J., Banyikwa, F., Bronn, A., Bucini, G., Caylor, K.K., Coughenour, M.B., Diouf, A., Ekaya, W., Feral, C.J., February, E.C., Frost, P.G.H., Hiernaux, P., Hrabar, H., Metzger, K.L., Prins, H.H.T., Ringrose, S., Sea, W., Tews, J., Worden, J., Zambatis, N., 2005. Determinants of woody cover in African savannas. Nature 438, 846–849. https://doi.org/10.1038/nature04070.
- Scheller, R.M., Domingo, J.B., Sturtevant, B.R., Williams, J.S., Rudy, A., Gustafson, E.J., Mladenoff, D.J., 2007. Design, development, and application of LANDIS-II, a spatial landscape simulation model with flexible temporal and spatial resolution. Ecol. Modell. 201, 409–419. https://doi.org/10.1016/j.ecolmodel.2006.10.009.
- Scholtz, R., Fuhlendorf, S.D., Uden, D.R., Allred, B.W., Jones, M.O., Naugle, D.E., Twidwell, D., 2021. Challenges of Brush Management Treatment Effectiveness in Southern Great Plains, United States. Rangeland Ecology & Management 77, 57–65. https://doi.org/10.1016/j.rama.2021.03.007.
- Shabani, F., Kumar, L., Ahmadi, M., 2016. A comparison of absolute performance of different correlative and mechanistic species distribution models in an independent area. Nat. Ecol. Evol. 6, 5973–5986. https://doi.org/10.1002/ece3.2332.
- Sillmann, J., Kharin, V.V., Zwiers, F.W., Zhang, X., Bronaugh, D., 2013. Climate extremes indices in the CMIP5 multimodel ensemble: Part 2. Future climate projections. J. Geophys. Res. Atmos. 118, 2473–2493. https://doi.org/10.1002/jgrd.50188.
- Stevens, N., Lehmann, C.E.R., Murphy, B.P., Durigan, G., 2017. Savanna woody encroachment is widespread across three continents. Global Change Biol. 23, 235–244. https://doi.org/10.1111/gcb.13409.
- Taylor, K.E., Stouffer, R.J., Meehl, G.A., 2012. An Overview of CMIP5 and the Experiment Design. Bull. Am. Meteorol. Soc. 93, 485–498. https://doi.org/10.1175/BAMS-D-11-00094.1.
- Thompson, S.J., Arnold, T.W., Amundson, C.L., 2014. A multiscale assessment of tree avoidance by prairie birds. The Condor 116, 303–315. https://doi.org/10.1650/ CONDOR-13-072.1.
- Thuiller, W., Georges, D., Gueguen, M., Engler, R., Breiner, F., Lafourcade, B., Patin, R., 2023. biomod2: Ensemble Platform for Species Distribution Modeling. R package version 4.2-5.
- Torquato, P.R., Will, R.E., Zhang, B., Zou, C.B., 2020a. Stand-Level Transpiration Increases after Eastern Redcedar (Juniperus virginiana L.) Encroachment into the Midstory of Oak Forests. Forests 11, 901. https://doi.org/10.3390/f11090901.
- Torquato, P.R., Zou, C.B., Adhikari, A., Adams, H.D., Will, R.E., 2020b. Drought Tolerance and Competition in Eastern Redcedar (Juniperus virginiana) Encroachment of the Oak-Dominated Cross Timbers. Front. Plant Sci. 11.
- Twidwell, D., Fuhlendorf, S.D., Taylor Jr, C.A., Rogers, W.E., 2013a. Refining thresholds in coupled fire–vegetation models to improve management of encroaching woody plants in grasslands. J. Appl. Ecol. 50, 603–613. https://doi.org/10.1111/1365-2664.12063.
- Twidwell, D., Rogers, W.E., Fuhlendorf, S.D., Wonkka, C.L., Engle, D.M., Weir, J.R., Kreuter, U.P., Taylor Jr, C.A., 2013b. The rising Great Plains fire campaign: citizens' response to woody plant encroachment. Front. Ecol. Environ. 11, e64–e71. https://doi.org/10.1890/130015.
- Twidwell, D., Wonkka, C.L., Taylor Jr, C.A., Zou, C.B., Twidwell, J.J., Rogers, W.E., 2014. Drought-induced woody plant mortality in an encroached semi-arid savanna depends on topoedaphic factors and land management. Appl. Veg. Sci. 17, 42–52. https://doi.org/10.1111/avsc.12044.
- Venter, Z.S., Cramer, M.D., Hawkins, H.J., 2018. Drivers of woody plant encroachment over Africa. Nat. Commun. 9, 2272. https://doi.org/10.1038/s41467-018-04616-8.
- Wang, J., Xiao, X., Qin, Y., Doughty, R.B., Dong, J., Zou, Z., 2018. Characterizing the encroachment of juniper forests into sub-humid and semi-arid prairies from 1984 to 2010 using PALSAR and Landsat data. Remote Sens. Environ. 205, 166–179. https://doi.org/10.1016/j.rse.2017.11.019.
- Wei, B., Wang, R., Hou, K., Wang, X., Wu, W., 2018. Predicting the current and future cultivation regions of Carthamus tinctorius L. using MaxEnt model under climate change in China. Glob. Ecol. Conserv. 16, e00477. https://doi.org/10.1016/j.gecco.2018.e00477.
- Westerling, A.L., Gershunov, A., Brown, T.J., Cayan, D.R., Dettinger, M.D., 2003. Climate and Wildfire in the Western United States. Bull. Am. Meteorol. Soc. 84, 595–604. https://doi.org/10.1175/BAMS-84-5-595.

- Wilcox, B.P., Birt, A., Archer, S.R., Fuhlendorf, S.D., Kreuter, U.P., Sorice, M.G., van Leeuwen, W.J.D., Zou, C.B., 2018. Viewing Woody-Plant Encroachment through a Social–Ecological Lens. Bioscience 68, 691–705. https://doi.org/10.1093/biosci/ biy051.
- Wilcox, B.P., Fuhlendorf, S.D., Walker, J.W., Twidwell, D., Wu, X.B., Goodman, L.E., Treadwell, M., Birt, A., 2022. Saving imperiled grassland biomes by recoupling fire and grazing: a case study from the Great Plains. Front. Ecol. Environ. 20, 179–186. https://doi.org/10.1002/fee.2448
- Yamazaki, D., Ikeshima, D., Tawatari, R., Yamaguchi, T., O'Loughlin, F., Neal, J.C., Sampson, C.C., Kanae, S., Bates, P.D., 2017. A high-accuracy map of global terrain elevations. Geophys. Res. Lett. 44, 5844–5853. https://doi.org/10.1002/2017GL072874.
- Yang, J., Tian, H., Tao, B., Ren, W., Pan, S., Liu, Y., Wang, Y., 2015. A growing importance of large fires in conterminous United States during 1984–2012.
  - J. Geophys. Res. 120, 2625-2640. https://doi.org/10.1002/2015JG002965.
- Yang, J., Zou, C., Will, R., Wagner, K., Ouyang, Y., King, C., Winrich, A., Tian, H., 2023. River flow decline across the entire Arkansas River Basin in the 21st century. J. Hydrol. 618, 129253 https://doi.org/10.1016/j.jhydrol.2023.129253.
- Yang, X., Xiao, X., Zhang, C., 2023. Spatiotemporal variability and key factors of evergreen forest encroachment in the southern Great Plains. J. Environ. Manage. 329. 117012 https://doi.org/10.1016/j.jenyman.2022.117012.
- Zhou, Y., Zhang, Z., Zhu, B., Cheng, X., Yang, L., Gao, M., Kong, R., 2021. MaxEnt Modeling Based on CMIP6 Models to Project Potential Suitable Zones for Cunninghamia lanceolata in China. Forests 12, 752. https://doi.org/10.3390/f12060752.
- Zou, C.B., Twidwell, D., Bielski, C.H., Fogarty, D.T., Mittelstet, A.R., Starks, P.J., Will, R. E., Zhong, Y., Acharya, B.S., 2018. Impact of Eastern Redcedar Proliferation on Water Resources in the Great Plains USA—Current State of Knowledge. Water 10, 1768. https://doi.org/10.3390/w10121768.